# rss_ringoccs: User Guide
## V1.3

©Team Cassini at Wellesley College
Richard G. French[*], Sophia R. Flury, Jolene W. Fong,
Ryan J. Maguire, and Glenn J. Steranka

[*]*Cassini Radio Science Team Leader,*
*rfrench@wellesley.edu*

August 28, 2019

# Contents

# List of Figures

# List of Tables

$$\hat{T} = \int_a^\infty \exp(i\psi)d\rho \qquad (1)$$

$$\theta_{shift} = \tan^{-1}\left(\frac{\Im(\hat{T}(\rho - \rho_{shift}))}{\Re(\hat{T}(\rho - \rho_{shift}))}\right) \qquad (2)$$

$$\hat{T}_{echo} = \int_a^\infty \exp(i\theta_{shift})\exp(i\psi)d\rho \qquad (3)$$

$$T = \int_{-\infty}^\infty \hat{T}_{echo}\exp(-i\psi)d\rho_0 \qquad (4)$$

$$\hat{T}_{echo} = \int_a^\infty \exp(i(\theta_{shift} + \theta))\exp(i\psi)d\rho \qquad (5)$$

# 1 Introduction

The Cassini Radio Science Subsystem (RSS) was used during the Cassini orbital tour of Saturn to observe a superb series of ring occultations that resulted in high-resolution, high-SNR radial profiles of Saturn's rings at three radio wavelengths: 13 cm (S band), 3.6 cm (X band), and 0.9 cm (Ka band). Radial optical depth profiles of the rings at 1- and 10-km resolution produced by Essam Marouf of the Cassini RSS team, using state-of-the-art signal processing techniques to remove diffraction effects, are available on the NASA Planetary Data System (PDS).[1] These archived products are likely to be quite adequate for many ring scientists, but for those who wish to generate their own diffraction-reconstructed ring profiles from Cassini RSS observations, we provide `rss_ringoccs`: a suite of Python-based analysis tools for radio occultations of planetary rings.[2]

The purpose of `rss_ringoccs` is to enable scientists to produce "on demand" radial optical depth profiles of Saturn's rings from the raw RSS data, without requiring deep familiarity with the complex processing steps involved in calibrating the data and accounting for the effects of diffraction. The code and algorithms are extensively documented, providing a starting point for users who wish to test, refine, or optimize the straightforward methods we have employed. Our emphasis has been on clarity, sometimes at the expense of programming efficiency and execution time. `rss_ringoccs` does an excellent job of reproducing existing RSS processed ring occultation data already present on NASA's PDS Ring-Moon Systems Node – detailed comparisons of representative examples of our results with those on the PDS are presented below in Section 5.1. However, we make no claim to having achieved the state-of-the-art in every respect. In a project this complex, bugs may well be present, and we encourage users to report any errors, augment our algorithms, and share these improvements so that they can be incorporated in future editions of `rss_ringoccs`.

This document provides an introduction to RSS ring occultations, directs users to required and recommended reading, describes in detail how to set up `rss_ringoccs`, and explains how to obtain RSS data files and auxiliary files required by the software. It provides an overview of the processing pipeline, from raw data to final high-resolution radial profiles of the rings, and guides users through a series of simple examples to illustrate the use of `rss_ringoccs`. The algorithms and code are validated by comparison with Voyager and Saturn RSS results on the PDS archive, and with analytical results. Finally, it includes practical considerations for users, and benchmarks of program execution time.

## 1.1 Getting help

`rss_ringoccs` is easy to install and use, but if you have questions along the way please don't hesitate to get in touch with us. We recommend that you post an issue to the `rss_ringoccs` repository[3] so that other users can join in the conversation, but you are also free to contact the lead author of the project, Richard G. French, at *rfrench@wellesley.edu*. For reference, we provide detailed documentation of the software online at https://rss-ringoccs.readthedocs.io/en/master/.

---

[1] https://pds-rings.seti.org/cassini/rss/index.html

[2] `rss_ringoccs` may be found from https://github.com/NASA-Planetary-Science/rss_ringoccs

[3] https://github.com/NASA-Planetary-Science/rss_ringoccs/issues

## 1.2 What is an RSS ring occultation?

In its simplest form, an RSS ring occultation occurs when a radio signal transmitted from a spacecraft's High Gain Antenna (HGA) passes through the rings on the way to a Deep Space Network (DSN) receiving antenna on Earth. The received signal at Earth is affected by interactions of the radio signal with the swarm of ring particles, including attenuation, scattering, Doppler-shifting of the signal, and diffraction. We refer to the process of compensating for diffraction to obtain the intrinsic radial optical depth profile of the rings as diffraction reconstruction or Fresnel inversion, since the reconstruction process is based on the mathematical principles of Fresnel optics.

## 1.3 Overview of Cassini RSS ring observations

Over the course of the Cassini orbital tour of Saturn, the geometry of RSS ring occultations varied due to changes in the orbiter's trajectory and in the aspect of the rings as seen from Earth during Saturn's orbit around the Sun. The opening angle of Saturn's rings as a function of time as seen from Earth is shown below in **Fig. 1**.
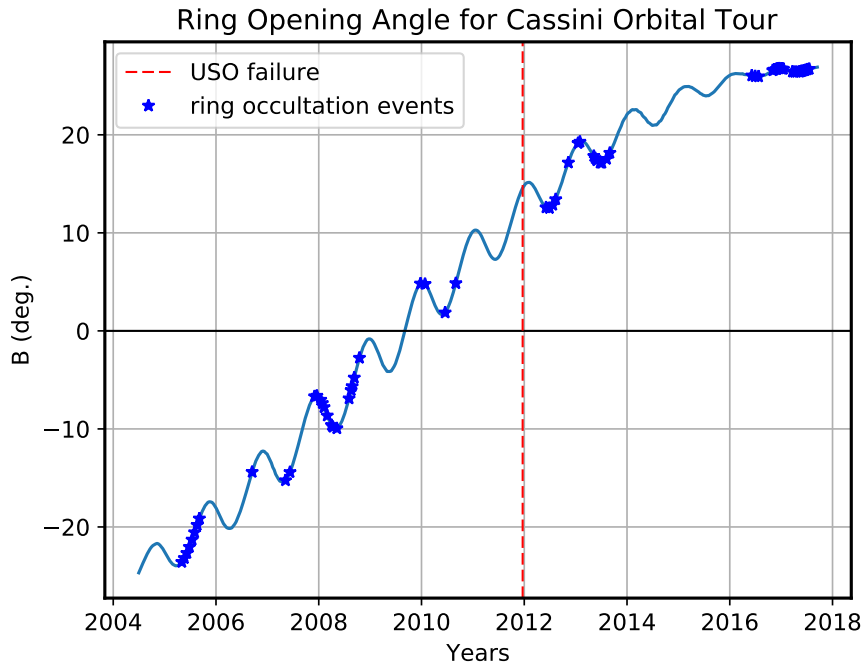


Fig. 1: Ring Opening angle ($B$) vs. Time. The rings are edge-one for an opening angle of $B = 0$. In 2012, the on-board ultra-stable oscillator (USO) failed, complicating diffraction reconstruction thereafter. Symbols mark the time and ring opening angle for individual Cassini RSS ring observations.

Individual occultations are identified by the Cassini rev number $n$, corresponding roughly to the $n^{\text{th}}$ orbit of Cassini around Saturn, during which the occultation occurred. During the ingress portion of an occultation, the orbital radius of the intercept point in the ring plane of the incident ray from the spacecraft decreases with time; the radius increases with time during the egress portion of an occultation. During a diametric occultation, the ingress and egress portions of the occultation are interrupted by passage of the spacecraft behind the planet itself as seen from Earth, resulting in an atmospheric occultation. For the Grand Finale orbits of the Cassini mission, the spacecraft trajectory was changed,

resulting in periapse being between the rings and Saturn. On these orbits, there were up to three separate ring occultations: a rapid egress 'proximal' occultation when the spacecraft was in front of the planet as viewed from Earth, followed by a more traditional chord occultation with an ingress and egress part, as the spacecraft receded from Earth behind the rings. The view from Earth of the ingress and egress portions of a diametric occultation on Rev 7 is shown in **Fig. 2.1**. During a chord occultation, the ingress and egress occultations are contiguous. The Earth view of the chord occultation on Rev 54 is shown in **Fig. 2.2**.



|  |  |
| :---: | :---: |
| 2.1: Rev007 | 2.2: Rev054 |
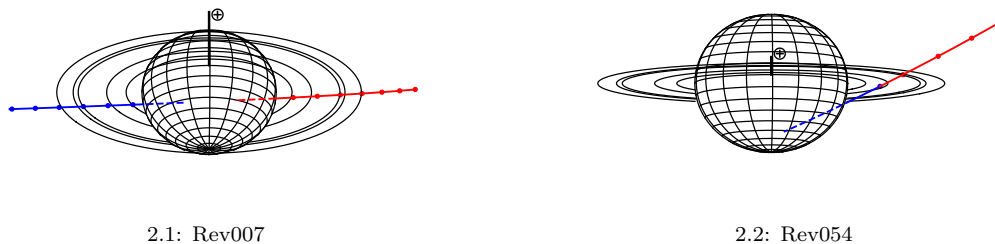
Fig. 2: Earth view of Cassini during the Rev007 and Rev054 ring occultation observations. The red solid lines represent the ingress portion of an occultation and the blue solid lines represent the egress portion. The blue and red dashed lines are the part of the occultation that is blocked by Saturn.

## 1.4 Cassini RSS ring occultation observations on NASA's PDS

There are two categories of Cassini RSS observations on the PDS: raw data in Radio Science Receiver (RSR) files that contain the digitized spacecraft signal as received at the DSN, and higher-level products (reduced data) that have been processed by the RSS team, including diffraction-reconstructed radial profiles of the optical depth of Saturn's rings and associated geometric and calibration information. rss_ringoccs processes raw RSR files and independently produces higher-level products that can be saved as files similar in form and content to those already on the PDS, but with a user-defined radial resolution.

### 1.4.1 Raw RSS data files

The raw data produced by the DSN that contain the original observations of all Cassini occultation observations are recorded in RSR files, described in more detail in the *Cassini Radio Science Users Guide* (Section 1.5.1). During Cassini RSS occultations, RSR files were typically recorded at two bandwidths: 1 kHz and 16 kHz – both types are available on the PDS for nearly all Cassini RSS ring experiments. The rss_ringoccs package can handle either version and they give nearly identical results, although the processing time for the 16 kHz files is significantly longer. We provide convenient scripts in rss_ringoccs (Section 2.4.2) to download both 1 kHz and 16 kHz RSR files before USO failure from the PDS archive. The 1 kHz files are preferred for nearly all cases; the 16 kHz files are required in cases where very high spatial resolution is desired.

### 1.4.2 Higher-level products

Essam Marouf of the Cassini RSS science team has produced a comprehensive set of set of higher-level products for ring occultation observations, available at https://pds-rings.

`seti.org/viewmaster/volumes/CORSS_8xxx/CORSS_8001`. This archive set contains 1- and 10-km resolution diffraction-reconstructed profiles from S-, X- and Ka-band observations of Revs 7 through 137. *Users interested in low-resolution ($\simeq 10$ km) ring profiles are advised to use the existing PDS results, rather than to use* `rss_ringoccs` *to produce them, since our software package does not implement the low-pass filtering techniques used for the PDS results to obtain the 10 km resolution profiles.*

## 1.5 Required and recommended reading

With this overview of RSS ring occultation observations and data in hand, we strongly recommend that all users familiarize themselves with several key documents before using the `rss_ringoccs` package. Our internal documentation of the `rss_ringoccs` code makes frequent reference to the following two documents:

### 1.5.1 Cassini Radio Science User's Guide

The most complete practical introduction to Cassini RSS ring observations is contained in the *Cassini Radio Science User's Guide*[4] (Asmar et al. 2018). We regard this as *required reading*. Chapter 2 describes the *open-loop* RSR files that contain the raw RSS ring occultation data, and Chapter 3.3 summarizes the analysis steps to produce a diffraction reconstruction ring optical depth profile from the observations. *For the remainder of this guide, we will assume that all readers have familiarized themselves with this material.*

### 1.5.2 Marouf, Tyler, and Rosen (1986) - MTR86

The definitive reference for diffraction reconstruction of RSS occultations is Marouf et al. 1986: Marouf, Tyler and Rosen's classic "Profiling Saturn's rings by radio occultation." We refer to this as MTR86. For copyright reasons, we cannot include MTR86 in this GitHub repository, but we highly recommend that scientists making use of radio occultation data have this paper readily at hand. It documents the Fresnel inversion method of diffraction reconstruction, complete with application to Voyager RSS occultation observations of Saturn's rings. This is *recommended reading* for beginning users of `rss_ringoccs`, and *required reading* for anyone wishing to understand the inner workings of the `rss_ringoccs` software package.

### 1.5.3 Online Documentation

Online documentation of `rss_ringoccs` functions, scripts, and modules can be found at `https://rss-ringoccs.readthedocs.io/en/master/`.

### 1.5.4 For more information...

Readers interested in an overview of Cassini RSS instrumentation and science goals are encouraged to read "Cassini Radio Science" by Kliore et al. 2004. Scientific results making use of Cassini RSS occultation observations include Colwell et al. 2009, Moutamid et al. 2016, French et al. 2016a, French et al. 2016b, French et al. 2017 Marouf et al. 2011,

---

[4]Available from `https://pds-rings.seti.org/cassini/rss/`

Nicholson et al. 2014a, Nicholson et al. 2014b, Rappaport et al. 2009, and Thomson et al. 2007.

# 2  Setting things up

This section provides step-by-step instructions for setting up the `rss_ringoccs` package and associated data files. We assume that all users are familiar with basic unix commands and introductory-level Python.

## 2.1  System requirements

The `rss_ringoccs` repository has been developed and tested on the following hardware, unix-based operating systems, and shells:

| Hardware | Operating System | Shell | GB of RAM |
|---|---|---|---|
| MacBookPro, iMac | MacOS 10.13.4, 10.14.5 | bash | 8, 16, and 32 |
| Mac mini | Linux Ubuntu Budgie 16 | bash | 8 |
| MacBookPro | Linux Ubuntu 16 | bash | 8 |
| ThinkMate | Linux Debian | bash | 32 |

Table 1: Hardware and operating systems

We strongly recommend that users run `rss_ringoccs` on a system with at least 16 GB of RAM (preferably 32 GB) to minimize disk-based memory swapping, which can significantly increase the run time when processing an entire occultation at high resolution.

## 2.2  Downloading the `rss_ringoccs` repository from GitHub

To download via `git clone`, open a terminal window and navigate to the directory below which you wish to install `rss_ringoccs` and type the command:

```
git clone https://github.com/NASA-Planetary-Science/rss_ringoccs.git
```

To download `rss_ringoccs` via ZIP file, visit
https://github.com/NASA-Planetary-Science/rss_ringoccs and click on the green *Clone or Download* pull-down menu at the upper right and click on *Download ZIP*. `rss_ringoccs-master.zip` will appear in your local `Downloads` directory; unzip it and move it to your desired directory. Unzipping the file will create an `rss_ringoccs-master` folder, as opposed to the `rss_ringoccs` folder that appears when the repository is downloaded using `git clone`.

## 2.3  Install Python 3 and required packages

`rss_ringoccs` has been developed under Python 3, in particular Python 3.5, 3.6, and 3.7. Our code has been tested under the following Python configurations:

| Operating System | Distribution | Version | URL |
|---|---|---|---|
| MacOS 10.14.1 | Anaconda | 3.6.3 | https://www.anaconda.com |
| MacOS 10.14.2 | Anaconda | 3.7.1 | https://www.anaconda.com |
| MacOS 10.14.5 | Anaconda | 3.6.8 | https://www.anaconda.com |
| Linux Ubuntu Budgie 16 | Anaconda | 3.6.3 | https://www.ubuntu.com |
| Linux Ubuntu 18 | Anaconda | 3.6.3 | https://www.ubuntu.com |
| Linux Debian | Anaconda | 3.6.3 | https://www.debian.org |

Table 2: Python versions compatible with `rss_ringoccs`

Once the `rss_ringoccs` package has been downloaded, the user will need to install Python 3 and various dependencies. The easiest way to do this by running the setup script `rss_ringoccs_config.sh`, included in the download. This will install Python 3 using Anaconda, as well as all of the necessary packages, and update and source the `.bash_profile` and `.bashrc` files. For users who have already installed Python, this script will update `conda` and then check that `spiceypy` and other packages exist on the machine. To run the setup script, navigate to the `rss_ringoccs` directory in a terminal and run the following:

```
./rss_ringoccs_config.sh
```

The installation process will begin, and may take several minutes. By default, the Anaconda3 distribution should contain ipython, an enhanced interactive Python shell. If it is absent, type the following command:

```
pip install ipython
```

ipython is useful for retaining a history of interactive Python commands and a host of other benefits. See https://ipython.readthedocs.io/en/stable/index.html for details.

If the configuration script fails in some fashion, or expected packages are not loaded, the user may instead manually install Python 3 and the required packages by visiting the URLs found in Table 2. A manual installation of Anaconda3 will provide all required dependencies, with the exception of the `spiceypy` package.

### 2.3.1  Download and install `spiceypy`

`rss_ringoccs` makes extensive use of JPL's NAIF SPICE toolkit (Acton 1996), a set of software tools to calculate planetary and spacecraft positions, ring occultation geometry, and a host of useful calendar functions.[5] Our software requires `spiceypy`, a Pythonized version of the NAIF toolkit, available from https://github.com/AndrewAnnex/SpiceyPy. The setup bash script detailed before should install `spiceypy` automatically, but `spiceypy` can also be installed manually by following the instructions on https://spiceypy.readthedocs.io/en/master/installation.html.

### 2.3.2  Test `spiceypy`

To test your installation of `spiceypy`, fire up Python in a terminal at the unix command line and at the `>>>` prompts, enter the following commands to confirm that `spiceypy`

---

[5]See https://naif.jpl.nasa.gov/naif/index.html

returns $\pi$ and the speed of light $c$:

```
python
>>> import spiceypy
>>> print(spiceypy.pi(),spiceypy.clight())
3.141592653589793 299792.458
>>> exit()
```

## 2.4   Downloading necessary files

`rss_ringoccs` provides bash-based shell scripts to automate the retrieval of necessary files. For quick setup and testing (Section 3.3) purposes, run the following command in the `examples` directory:

```
./get_example_files.sh
```

For more shell scripts to retrieve a complete list of files and a detailed explanation of their contents, see below.

### 2.4.1   JPL/NAIF SPICE kernels

The `rss_ringoccs` package makes extensive use of SPICE data (*kernel* files) from JPL/-NAIF that specify planetary and spacecraft ephemerides, planetary constants, and other essential information for computing the geometric circumstances of occultations.[6]  The `rss_ringoccs` distribution contains bash-based shell scripts to automate the retrieval of SPICE kernels from the NAIF website and store them in subdirectories under `rss_ringoccs/kernels/`, following the same directory structure as on the NAIF ftp site. Some of the kernel files are quite large, and will take some time (and significant disk space) to download. The size of the total set of kernel files is 878 MB, so be sure that there is sufficient disk space available.

In order to compute the geometry of RSS occultations throughout the Cassini orbital tour, download a complete set of kernels by navigating to the `pipeline` directory and entering the following command:

```
./get_all_kernels.sh
```

The shell script detects whether a given kernel has already been downloaded, so you may interrupt this command if it hasn't run to completion in the time you have available, and repeat the command later, picking up the downloading process where it left off the previous time. However, if you stop the `get_kernels.sh` script while it is downloading a file, the file may be incomplete but will still be detected by future runs of the shell scripts as having been downloaded. You will need to delete incomplete files to restart the download. To check for incomplete files, look in the `lsk`, `pck`, and `spk` directories within the `rss_ringoccs/kernels/naif/CASSINI/kernels/` directory and in the `rss_ringoccs/kernels/naif/generic/kernels/` directory. The most likely incomplete files will be `.bsp` files located in the `spk/` directory where kernel files for each occultation set of spacecraft and planetary ephemerides are stored; however, it is best to check all kernel directories.

---

[6]For detailed information about kernels, visit https://naif.jpl.nasa.gov/naif/data.html

Once you have downloaded the complete set of kernels, you will not need to repeat this process unless JPL releases an updated set of Cassini trajectory files. We plan to update this documentation and the input files for `get_kernels.sh` if that occurs. The meta-kernel for the total set of Cassini and Saturn kernels is located in `../tables/e2e_kernels.ker`, which the user will need to reference when running `rss_ringoccs`.

### 2.4.2 Cassini RSS raw data files

The `rss_ringoccs` package requires local access to raw Cassini RSS data files (Section 1.4.1). The storage capacity on GitHub is not sufficient to allow even one sample RSR file to be part of the standard download. We provide scripts to download three separate sets of RSR files. These can be called by navigating to the `rss_ringoccs/pipeline` directory and executing the scripts as shown here:

```
cd rss_ringoccs/pipeline
./get_1kHz_rsr_files_preUSOfailure.sh
./get_1kHz_rsr_files_postUSOfailure.sh
./get_16kHz_rsr_files_preUSOfailure.sh
```

These will take quite some time to execute (up to several hours, depending on internet speed), given the large data volume (10 GB for just the pre-USO failure 1 kHz RSR files) to be transferred over the internet. Note that the following eight files on the PDS differ in name from the files used in `CORSS_8001`:

| CORSS_8001 file | PDS file |
| --- | --- |
| S10EAOE2005_123_0740NNNK34D.1B1 | S10SROE2005123_0740NNNK34RD.1B1 |
| S10EAOE2005_123_0740NNNS43D.2B1 | S10SROE2005123_0740NNNS43RD.2B1 |
| S10EAOE2005_123_0740NNNX34D.1A1 | S10SROE2005123_0740NNNX34RD.1A1 |
| S10EAOE2005_123_0740NNNX43D.2A1 | S10SROE2005123_0740NNNX43RD.2A1 |
| S10EAOC2005_123_0229NNNS43D.2B1 | S10SROI2005123_0230NNNS43RD.2B1 |
| S12SROE2005177_2226NNNX14RD.2A1 | S12SROE2005177_2225NNNX14RD.2A1 |
| S12SROI2005177_1745NNNS14RD.2B1 | S12SROI2005177_1740NNNS14RD.2B1 |
| S12SROI2005177_1745NNNX14RD.2A1 | S12SROI2005177_1740NNNX14RD.2A1 |

Table 3: PDS RSR file name changes

In addition, there are three 1 kHz files used by `CORSS_8001` that are currently not available on the PDS. In `../tables/rsr_1kHz_files_before_USO_failure.txt`, we replace these missing files with their 16 kHz equivalents, shown in Table 4.

| 1 kHz missing from PDS | 16 kHz version |
| --- | --- |
| S10EAOI2005_123_0230NNNK26D.3B1 | s10sroi2005123_0230nnnk26rd.3b2 |
| S10EAOI2005_123_0230NNNX26D.3A1 | s10sroi2005123_0230nnnx26rd.3a2 |
| S10EAOC2005_123_0229NNNX43D.2A1 | s10sroi2005123_0230nnnx43rd.2a1 |

Table 4: Left: 1 kHz files processed in `CORSS_8001` that are currently unavailable on the PDS. Right: 16 kHz equivalent of the missing files. Names are case-sensitive.

`rss_ringoccs` is currently able to process all pre-USO failure files and a subset of the post-USO failure files. The latter observations were obtained in a novel "two-way" mode

utilizing the frequency stability of a maser at the DSN to transmit a signal to the space-craft that was then phase-locked and retransmitted to the ground. Since the uplink signal is phase-shifted by diffraction effects during its upward passage through the rings, this results in a time-shifted phase "echo" that corrupts the standard diffraction reconstruction process. Users interested in the post-USO failure results should contact Dick French (rfrench@wellesley.edu) for details, prior to using these files.

## 2.5   Hard drive space

As a part of the hardware requirements for using `rss_ringoccs`, we describe here the requisite hard drive space for running the software. Although the software itself is relatively small in size ($\lesssim$ 3 Mb), the files needed to produce science data products require a substantial amount of drive space. The full set of kernel files downloaded following Section 2.4.1 is 878 Mb in size. The full set of 1 kHz RSR files downloaded following Section 2.4.2 is 10.43 Gb in size. In total, the files required to process all occultations observed before USO failure at 1 kHz will require 11.35 Gb of drive space.

While this accounts for the initial space necessary for processing every pre-USO-failure occultation observation, the output files for each end-to-end pipeline data reduction will take up additional drive space. A single occultation (e.g., Rev 007 E X43) processed at 0.25 km diffraction-limited resolution and 1 km reconstruction resolution will produce $\approx$ 520 Mb of output files. The output files containing the DLP and reconstructed profiles (the DLP and TAU files, respectively, described in more detail below) are 61.2 Mb each when the profile covers the entire ring system, and these two output file types represent $> 90\%$ of the output file data volume. A smaller radial spacing / higher radial resolution will increase the output file size.

The duration of each occultation observation varies from rev to rev, depending on the occultation geometry and the elevation angle of Saturn relative to Earth's horizon at any given DSN station. Additionally, the number of frequency bands and DSN stations at which a given occultation is observed also vary. As such, any given RSR file may not yield a complete radial profile resulting in smaller DLP and TAU files. Processing all 1 kHz RSR files prior to USO failure (Section 3.5) will result in about 23 GB of output files.

## 2.6   Install A LaTeX compiler

To make full use of `rss_ringoccs`, you'll need a LaTeX compiler to create the summary PDF file produced for each data sets as part of the end-to-end processing pipeline. `rss_ringoccs` requires the pdflatex compiler. MacTeX contains all of the necessary packages and more, and is recommended for users of MacOSX who wish to use LaTeX to its full capacity. A download can be found at
https://www.tug.org/mactex/mactex-download.html. This is a very large download (a few GB). For users who want only the necessary compiler and associated binary files, Basictex will suffice. This can be downloaded from https://www.tug.org/mactex/morepackages.html. For linux users, enter one of the following commands:

```
sudo apt-get install texlive-full
```

or:

```
sudo apt-get install texlive-latex-base
```

This will again download either a plethora of packages for LaTeX and the necessary compiler, or simply the basic necessities. In an attempt to keep the LaTeX portion of the code simple, very few packages are used. A complete list, and how they appear in the code, is given as follows:

```
%--------------------Begin LaTeX Code--------------------%
\usepackage{geometry}
\geometry{a4paper, margin = 1.0in}
\usepackage{graphicx, float}
\usepackage{lscape}
\usepackage[english]{babel}
\usepackage[dvipsnames]{xcolor}
\usepackage[font={normalsize}, labelsep=colon]{caption}
```

In the event of a successful install of either package, all of these dependencies should now be available to the user. Should any error arise, a manual install can be done by visiting the CTAN website. For example, the `float` package can be found from https://ctan.org/pkg/float.

## 2.7   Installing GCC (C compiler) and compiling

As of v1.2, `rss_ringoccs` makes use of the Numpy-C API and has many of the functions written in C, with wrappers for use in Python. This is done by using what is called the universal functions API, or ufuncs for short. To use these functions one must be able to run the setup scripts, which require the use of `gcc`. Pre-compiled shared objects (.so files) are included in the `rss_ringoccs` GitHub repository that are compatible with MacOS, versions 10.12 and higher. Linux users will need to install `gcc` and run the setup scripts manually. Should one wish to edit the C code, it will need to be recompiled before it can be used. Thus it is worthwhile for Mac user's to install the compiler as well.

To install `gcc` on a Mac, one can simply install Xcode from the App store. A quick way to do this is to run the following command from a terminal window:

```
xcode-select --install
```

Be sure to accept the various terms and agreements that will be prompted. It is easy to miss these and may result in a failed install. For Ubuntu 18, the command is:

```
sudo apt install gcc
```

Similar commands exist depending on which package manager you are using. Once this is done, you can test that your compiler is working with the following simple code (Call it hello.c):

```
#include <stdio.h>

int main(){
    printf("Hello,␣World!\n");
    return 0;
}
```

Then compile as follows:

```
gcc hello.c -o hello
```

If your compiler has installed correctly, you should have an executable called `hello`. Running `./hello` should print a nice message. Now that you have a C compiler, navigate to the _ufuncs directory where all of the C code is located. This is found in `rss_ringoccs/rss_ringoccs/_ufuncs`. If you are a Linux user, you may want to remove all of the pre-compiled .so files. To compile, simply run the setup script:

```
./setup.sh
```

Progress messages should print out indicating that three separate source files were successfully compiled. There are two main possible sources for error in the step. The first is that there is something missing in the `rss_ringoccs/include` directory. This directory contains all of the header files necessary for using the Numpy-C API. Should an error occur, check your directory against the one available on the `rss_ringoccs` GitHub repository. A second common error is that the compiler can't find many of the additional required header files that are provided by Anaconda. Make sure that you are running bash, since the Anaconda setup script only sources the bash profile. Next make such that ∼`/anaconda3/bin` is in your `PATH` variable. If not, try running the `rss_ringoccs_config.sh` script again, or running a manual install of Anaconda.

To check that you have successfully compiled everything, try running Python or iPython and importing `rss_ringoccs`. A successful import should look as follows:

```
cd rss_ringoccs/pipeline
python
>>>import sys
>>>sys.path.append(../')
>>>import␣rss_ringoccs
```

A failed install will result in the following messages printing:

```
cd rss_ringoccs/pipeline
python
>>>import sys
>>>sys.path.append(../')
>>>import rss_ringoccs

    Error: rss_ringoccs.diffrec.window_functions
        Could Not Import C Code. Stricly Using Python Code.
        This is signicantly slower. There was most likely an error
        in your installation of rss_ringoccs. To use the C Code,
        download a C Compiler (GCC) and see the User's Guide for
        installation instructions.


    Error: rss_ringoccs.diffrec.special_functions
        Could Not Import C Code. Stricly Using Python Code.
        This is signicantly slower. There was most likely an error
        in your installation of rss_ringoccs. To use the C Code,
        download a C Compiler (GCC) and see the User's Guide for
```

```
        installation instructions.


   Error: rss_ringoccs.diffrec.diffraction_correction
        Could Not Import C Code. Stricly Using Python Code.
        This is signicantly slower. There was most likely an error
        in your installation of rss_ringoccs. To use the C Code,
        download a C Compiler (GCC) and see the User's Guide for
        installation instructions.

In [2]:
```

You will still be able to use `rss_ringoccs`, but at a significantly slower rate. Functions from the `special_functions` and `window_functions` submodule are more then 50 times faster in C than in Python, whereas the C versions of routines in the `diffraction_correction` submodule are faster by a factor ranging from 20 to 30, depending on the function.

# 3   Using `rss_ringoccs`

Here, we provide an overview for using `rss_ringoccs`, including requisite information for writing your own scripts to process the data as well as directions for running example scripts.

## 3.1   End-to-end pipeline outline

For those interested in the the high-level structure of the processing pipeline, we offer this brief overview. An end-to-end script will require instantiating five separate Python classes in succession:

1. `rsr_inst = rss.RSRReader('RSR_filename.a2a')`

   - Creates an instance of the `RSRReader` class and stores it in `rsr_inst`.

2. `geo_inst = rss.occgeo.Geometry(rsr_inst, planet, spacecraft, kernels)`

   - Creates an instance of the `Geometry` class and stores it in `geo_inst`.
   - Takes an `RSRReader` instance and user-specified planet, spacecraft, and kernel files.
   - Calculates, among other things, the radial intercept point $\rho$ where the Cassini spacecraft radio signal is occulted by the rings and the locations of gaps in the occultation profile.
   - Produces `GEO*.TAB` and `GEO*.LBL` files.
   - These and all subsequent output files are written to a user-specified output directory

3. `cal_inst = rss.calibration.Calibration(rsr_inst, geo_inst)`

   - Creates an instance of the `Calibration` class and stores it in the variable `cal_inst`

- Takes the `RSRReader` (`rsr_inst`) and `Geometry` (`geo_inst`) instances

- This instance contains the calibrations necessary to convert the raw data into a diffraction-limited radial ring profile

- Calculates the observed frequency of the spacecraft signal to correct the real and imaginary components of the transmittance ($I$ and $Q$), then estimates the intrinsic received power over the entire occultation

- Produces `CAL*.TAB` and `CAL*.LBL` files following the naming convention for the GEO files

- Produces frequency offset fit plots (`*FORFIT.PDF`) and free space power fit plots (`*FSPFIT.PDF`)

4. `dlp_inst = rss.calibration.DiffractionLimitedProfile(`

   `rsr_inst, dr, geo_inst, cal_inst)`

   - Creates an instance of the `DiffractionLimitedProfile` class and stores it in the variable `dlp_inst`.

   - Takes the `RSRReader`, `Geometry`, and `Calibration` instances.

   - Contains as attributes the DLP (DiffractionLimitedProfile) as calibrated and reduced by the previous classes

   - Optional input of radial sampling rate `dr_km_desired` in kilometers

   - Calculates the normalized power $P/P_0$ and the diffraction-limited optical depth profile assuming $\tau = -\sin B \ln(P/P_0)$

   - Produces `DLP*.TAB` and `DLP*.LBL` files with the same naming convention as the GEO and CAL files with the additional `RRRR` indicator containing the specified radial resolution.

5. `tau_inst = rss.diffrec.DiffractionCorrection( dlp_inst,res_km)`

   - Creates an instance of the `DiffractionCorrection` class and stores it in the variable `tau_inst`

   - takes the `DiffractionLimitedProfile` instance and a user-specified reconstruction resolution `res_km` in kilometers

   - Calculates the reconstructed radial optical depth profile by accounting for diffraction effects by means of Fresnel inversion at the user specified reconstruction resolution.

   - Produces `TAU*.TAB` and `TAU*.LBL` files following the same naming convention as the DLP files except that `RRRR` here indicates the reconstruction resolution selected by the user when instantiating the `DiffractionCorrection()` class

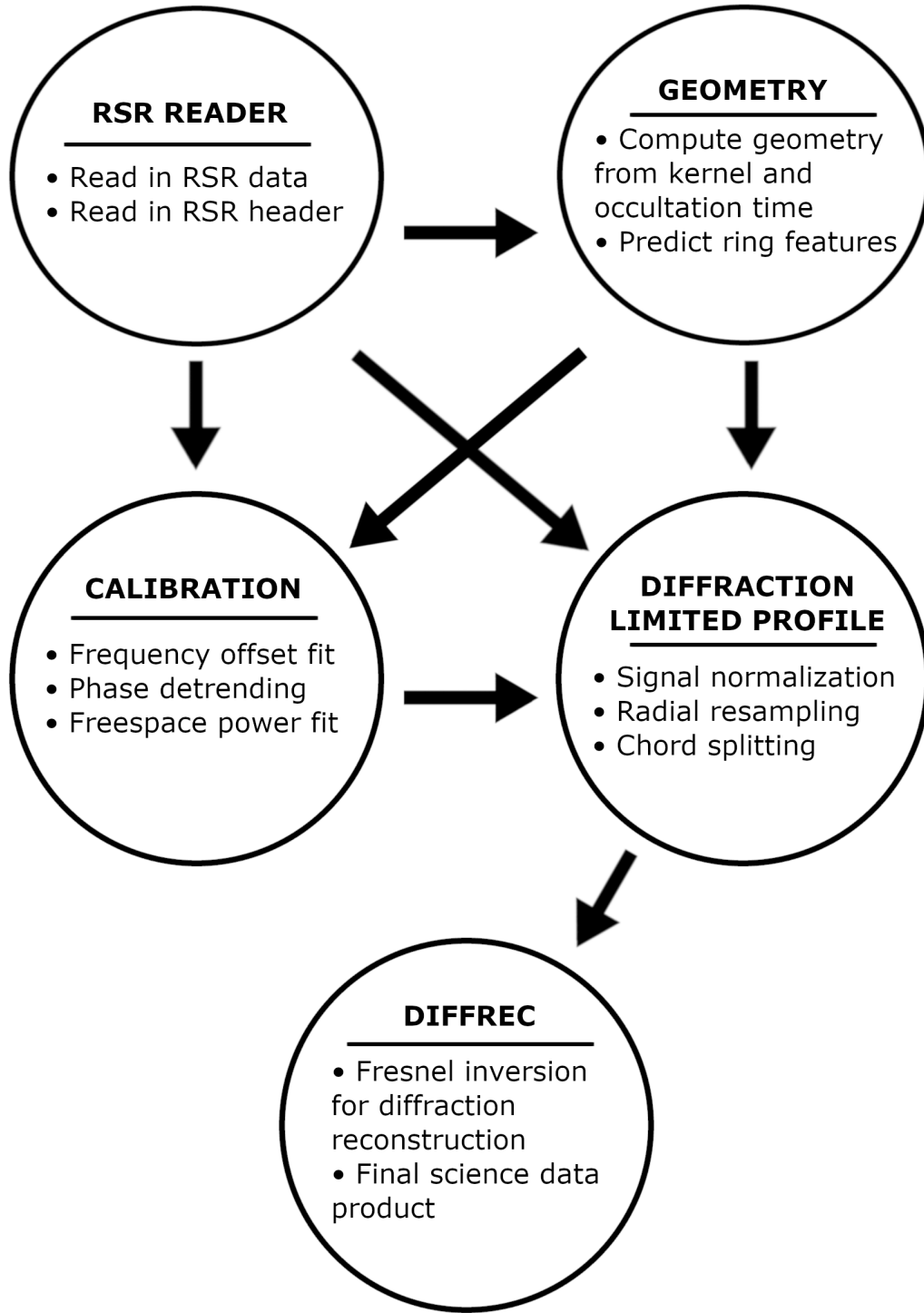Fig. 3: Data processing pipeline. Each bubble is a separate object called by the `e2e*.py` scripts.

## 3.2 Conventions and hierarchy

Here, we list some conventions used in the `rss_ringoccs` directory structure/hierarchy and the names of directories and output files.

- No reference is made within the `rss_ringoccs` package to local directories outside of the top-level `rss_ringoccs/` hierarchy of directories.

- The directory structure under `rss_ringoccs/` *must* strictly follow that of the original download from the GitHub repository.

- For portability, all references within `rss_ringoccs` software to pathnames to other directories within `rss_ringoccs/` are relative, not absolute.

- Unless otherwise noted, all executable scripts and Python programs *must* be run from within the `rss_ringoccs/pipeline/` directory. (This is so that relative pathnames will point to the correct directories.)

- Output file names follow the format:
  `RSS_OBSY_DOY_B##_D_INF_RRRRRM_YYYYMMDD_XXXX.EXT`

  ○ `OBSY` is the year the observation was made

  ○ `DOY` is the day of the year the observation was made

  ○ `B` is the wavelength band of the observation

  ○ `##` is the DSN station number

  ○ `D` is the direction of the occultation

  ○ `INF` is a three-letter reference specifying the information stored within the file (`GEO` for the occultation geometry, `FOF` for the frequency offset, `CAL` for calibration, `DLP` for the DLP, and `TAU` for the diffraction-reconstructed optical depth profile)

  ○ `YYYYMMDD` is the year, month, and date on which the user ran the `rss_ringoccs` code

  ○ `XXXX` is the *XXXX*th run of `rss_ringoccs` on that date

  ○ `EXT` is the file extension

  ○ Only DLP and TAU files contain the `RRRRR` in the filename. For the DLP files, `RRRRR` is the minimum reconstruction resolution (the so-called "DLP resolution" in MTR86) in meters while for TAU files this is the processing resolution selected by the user

  ○ The output LBL files match those from the PDS with minor changes.

With these caveats in mind, users are highly encouraged to write their own scripts to call upon and make full use of the `rss_ringoccs` package. To that end, we provide example scripts for both pipeline versions as well as specific portions of the pipeline.

## 3.3   End-to-end pipeline: A look at the Huygens ringlet

The "end-to-end" pipeline process is a set of steps that need to be performed only once when processing a given RSR file from scratch. For the initial run, users will need to supply an RSR file, a set of kernels to use, a radial spacing to resample to, and a reconstruction resolution (there are also default keyword inputs documented within each routine). The RSR extraction, geometry calculation, and frequency offset calculation steps are all automated; however, users may specify several options and parameters in advance by editing the input file `e2e_run_args.py` in the `./examples/` directory. These options include whether to process 16 kHz files, whether to write results to output files,

whether to send output to the terminal, and whether the pipeline should enter an interactive mode to customize the freespace power fitting. This interactive mode will display the automated fit results in a `matplotlib` plotting window and prompt the user for changes to the fit parameters and/or freespace regions.

At the end of the end-to-end run, if the `write_file` keyword argument is set to `True`, several data files will be generated: geometry files, calibration files, diffraction-limited profile files, reconstructed optical depth files, and a summary file (in PDF format). Each class instantiated in the end-to-end pipeline process corresponds to a specific set of output files that match the format of those on the PDS produced by Essam Marouf. Once these files have been produced, users can use the quick-look process for subsequent runs.

The pipeline's arguments file includes additional parameters for customizing the calibration steps and the profile ranges and resolutions. Detailed descriptions of which resolution values to choose and definitions of each type of resolution are given below.

The following script illustrates the end-to-end pipeline by producing a diffraction-corrected profile of Saturn's Huygens ringlet. To execute this script, follow the example below.

```
cd rss_ringoccs/examples
python e2e_run.py
```

This will automatically produce the multipanel plot shown in Fig. 4. The top row of plots show the raw power, optical depth, and phase profiles (i.e., the observed diffraction pattern) that were input to `DiffractionCorrection`, and the bottom row shows the reconstructed radial profiles in power, optical depth and phase.
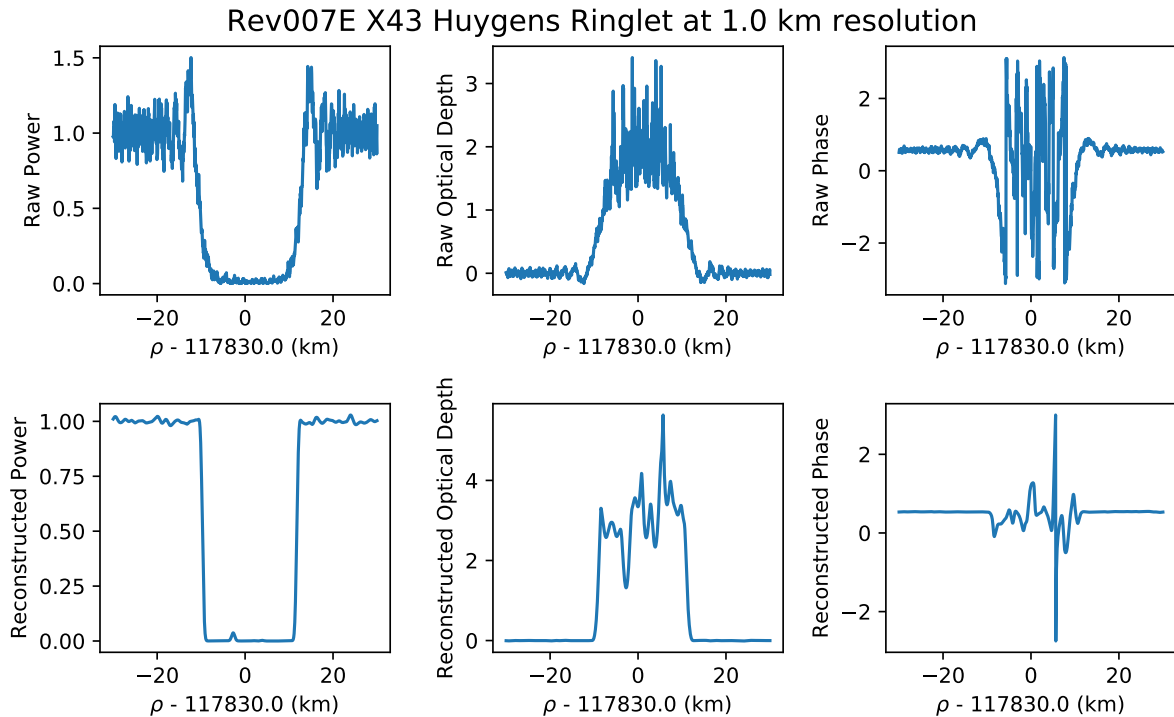


Fig. 4: Power, optical depth, and phase plots produced by e2e_run.py

## 3.4 Quick-look method: Comparing profiles reconstructed at different resolutions

The quick-look approach allows users to save computation time by utilizing pre-computed data files. For these runs, users start directly at the Fresnel inversion step of the pipeline, provided they have an appropriate set of `GEO*.TAB`, `CAL*.TAB`, and `DLP*.TAB` files. Users must specify the relative file path(s) and desired `*.TAB` files to the `tools.ExtractCSVData()` class to create a DLP instance similar to the one instantiated in the end-to-end pipeline from the `calibration.DiffractionLimitedProfile()` class. This DLP instance can then be passed to the `diffrec.DiffractionCorrection()` class.

Continuing with the RSR file downloaded in Section 2.4.2, we provide an example script to demonstrate diffraction-reconstructed optical depth profiles at different reconstruction resolutions for the Maxwell ringlet. Before running, users will need to open the `quick_look_run.py` script in a text editor and change line 15 from `date = 'YYYYMMDD'` to the date contained in the GEO, CAL, and DLP filenames. For the first set of Rev007 files output by the `e2e_run.py` script, this might resemble

```
date = '20190629'
data_dir = '../output/Rev007/Rev007E/Rev007E_RSS_2005_123_X43_E/'
geo_file = data_dir+'RSS_2005_123_X43_E_GEO_' + date + '_0001.TAB'
cal_file = data_dir+'RSS_2005_123_X43_E_CAL_' + date + '_0001.TAB'
dlp_file = data_dir+'RSS_2005_123_X43_E_DLP_0100M_'+date + '_0001.TAB'
```

To execute the example quick-look script, follow the example below"

```
cd rss_ringoccs/examples
python quick_look_run.py
```

This will produce optical depth profiles at four different reconstruction resolutions: 1 km, 0.75 km, 0.5 km, and 0.25 km for the Rev007 egress X-band observation from DSS-43 processed by the end-to-end script in Section 3.3. Running the script will produce a plot similar to Fig. 5 (not including the reference red line for PDS data).

## 3.5 Batch scripts

To simplify and expedite the use of `rss_ringoccs` to process large numbers of files, we provide a Python script `e2e_batch.py` in the `pipeline` directory that runs the end-to-end pipeline for a list of files contained in a reference ASCII text file. The default list, `rsr_1kHz_files_before_USO_failure.txt`, is the same list of files used by `get_rsr_files.sh` to download all of the 1 kHz Cassini RSR files prior to the USO failure, and can be found in the `tables/` directory. This batch script, like the single-file script, reads in a file of parameters, `e2e_batch_args.py`, which specifies, among other things, radial sampling rates, calibration fit orders, profile range, and whether to output files. By modifying the contents of `e2e_batch_args.py`, users can produce on-demand, customized optical depth profiles for specific data sets and radial regions of interest. Each option within `e2e_batch_args.py` is documented in comments. For more information, we refer users to either §4 or the documentation online at https: \rss-ringoccs.readthedocs.io.
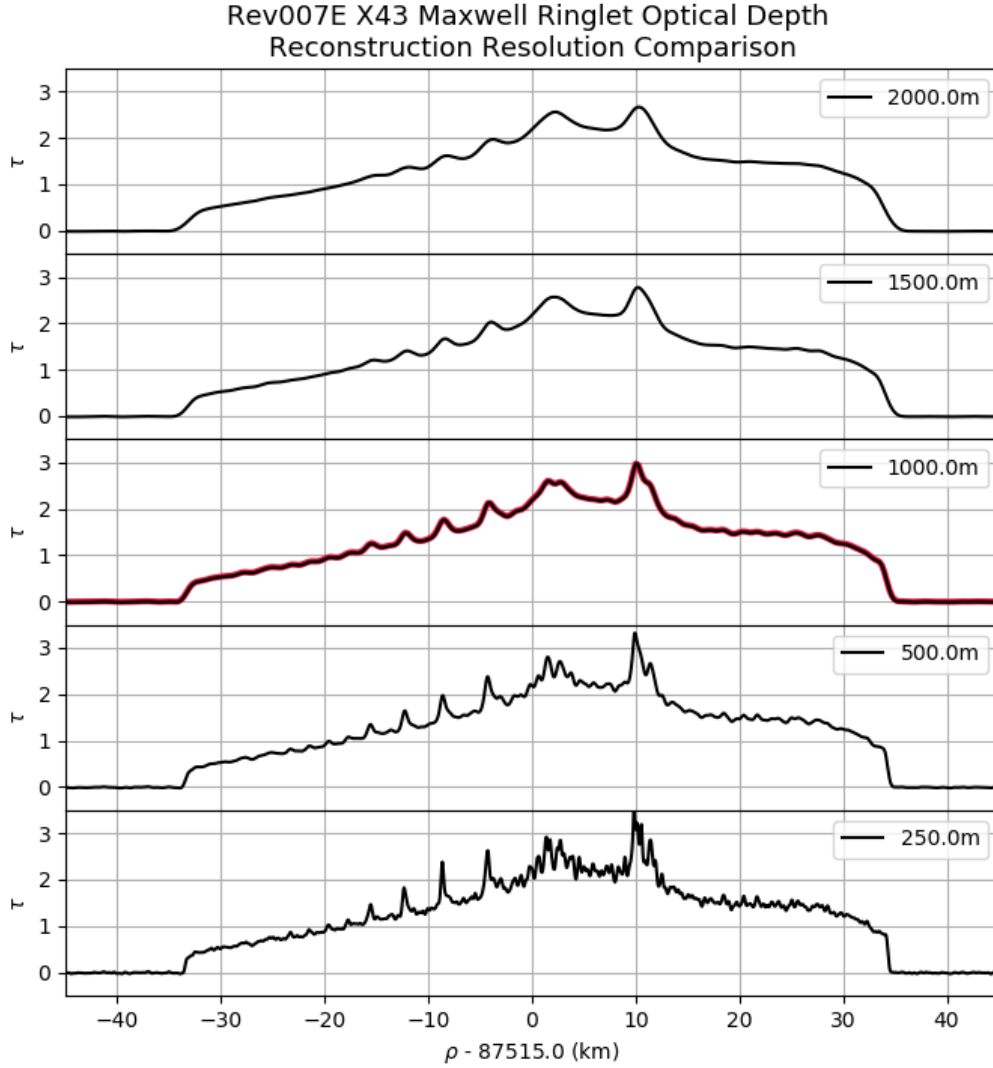
Fig. 5: Optical depth profile for the Maxwell ringlet from the Rev007E X43 occultation reconstructed at 2 km, 1 km, 0.5 km, and 0.25 km resolution. Solid black lines are the optical depth profile produced by the quick-look example script at various processing resolutions indicated by the plot text. For reference and validation, the solid red line is the 1 km reconstruction resolution profile obtained from the PDS3.

The default end-to-end pipeline will jump into its interactive mode when the automated normalization of the received power to a nominal free-space level is poor. To avoid this interactive mode, one can alternatively run the script prepended with the unix `yes` command to automatically enter the string "yes" for all input prompts (thus accepting the default fit, should `rss_ringoccs` enter interactive mode). Running the batch script in this manner will resemble

```
yes | python e2e_batch.py
```

The end-to-end Python script will automatically generate an error log file with a name such as `e2e_batch_YYYYMMDD-HHMMSS.err` to contain names of files that failed to process during the batch run as well as the resulting traceback error. If `verbose` keyword argument is set to `True`, some benign messages, such as:

19

```
1) WARNING (RSRReader): file size not the same as expected!
2) DETECTED INGRESS (resample_IQ.py): reversing arrays
```

will be printed to the terminal. These do not result in failed processing runs and are therefore not printed to the `.err` file.

One of the default parameters is `with16=False`, which skips 16 kHz files that have no corresponding 1 kHz files (see §2.4.2, Table 4). Set this to `True` only if the user's computer has at least 16 GB RAM; these files will also take longer to process than a typical 1 kHz file.

`rss_ringoccs` provides several additional end-to-end scripts to illustrate batch processing:

- From the `pipeline` directory, run this batch file for a 1 km reconstruction of occultations prior to USO failure. Execution time may vary with local hardware. Anticipate at least 3.5-4 hrs for this script to run.

  ```
  yes | python e2e_batch_1km.py
  ```

- From the `pipeline` directory, run this batch file for a 500 m reconstruction of occultations prior to USO failure. Execution time may vary with local hardware. Anticipate at least 15 hrs for this script to run.

  ```
  yes | python e2e_batch_500m.py
  ```

- For a 1 km reconstruction of occultations post-USO failure, run this batch file. Execution time may vary with local hardware. Anticipate at least 10 hrs for this script to run.

  ```
  yes | python e2e_batch_postUSO_1km.py
  ```

We strongly recommend that users not run simultaneous end-to-end batch jobs that use the same set of input RSR files, since this could result in inconsistent version numbers for the output files or overwriting/deletion of intermediate files that are normally hidden from the user.

## 3.6   Profile resolution

As a practical matter, most users would like to know: "What is the highest achievable resolution for a given ring occultation, and how can I use `rss_ringoccs` to produce a radial profile at that resolution?" The answer is complicated by a variety of definitions of resolution – we clarify these below – and is also affected of course by the SNR of any given occultation, which depends on the wavelength of the observation, the observing conditions at the DSN, the size of the receiving antenna, the geometry and speed of the occultation, and host of other factors.

We recommend that users begin with the 1-km reconstructions already available on the PDS, to get a sense for the signal quality of a specific occultation of interest. As a next step, we provide an end-to-end script that uses `rss_ringoccs` to process the entire set of Cassini RSS occultation data (up to the point of the USO failure) at a diffraction-corrected resolution of 0.5 km. Users can compare these profiles with the 1.0 km results available on the PDS, and decide whether reconstruction at a different resolution is needed.

In cases where higher resolution is desired and is warranted by the SNR, we recommend that `rss_ringoccs` users produce diffraction-reconstructed radial profiles at successively finer resolutions (centered on a feature of interest over a limited radial range to reduce processing time). As the resolution is increased, the effects of noise will eventually limit the useful information that can be obtained for a particular science goal.

To carry this out in practice, it is important to understand the factors that affect the diffraction-reconstructed resolution. Prior to diffraction reconstruction, RSS observations are limited in resolution at a spatial scale comparable to the Fresnel scale $F \approx \sqrt{\lambda D/2}$, where $\lambda$ is the wavelength of observation and $D$ is the distance between the spacecraft and the ring plane. Geometrical effects such as the tilt of the ring plane result in multiplicative scale factors applied to $F$, when converted to an effective diffraction-limited resolution in the radial direction in the ring plane. As a general rule, the effective Fresnel scale for RSS ring measurements is of order a few km for typical occultations.

The task of diffraction reconstruction is to improve on the diffraction-limited resolution of the observations by making use of both the intensity and phase of the received signal across the diffraction pattern. Intuitively, it makes sense that a high-resolution diffraction reconstruction will require finer resolution of the observed diffraction pattern, over a larger radial range (what we refer to as a *filter window* – see MTR86 for details), than a low-resolution reconstruction. For sub-km diffraction reconstruction at S-band (the longest of the three Cassini wavelengths), the filter window can extend for hundreds of km to either side of the location of the feature of interest, and it must be sampled at a fine enough spatial scale to capture the structure of fine-scale diffraction fringes produced by the ring feature over the entire filter window.

From these considerations, it is clear that in order to achieve a given post-reconstruction resolution, there is an implied requirement on the resolution at which the diffraction-limited profile is calculated. To satisfy the sampling theorem, if the radial sampling of the diffraction-limited DLP profile is $\Delta\rho$, the subsequent diffraction reconstruction resolution can only have shortest resolvable wavelengths of Nyquist or higher (i.e., $\geq 2\Delta\rho$) – more on this in a moment! As a practical matter, it sometimes makes sense to produce a DLP profile once and for all at very high resolution (say, 0.05 km), use it to produce a diffraction-reconstructed profile at, say, 1 km resolution, and then to reuse this same DLP profile to explore the SNR properties of successively higher resolution diffraction reconstructions, consistent with the sampling theorem.

The original data are recorded at regular intervals in time, but most of our processing is done as a function of ring plane radius. To achieve uniform radial sampling, we take account of the changing velocity and trajectory of the spacecraft and resam-

ple the phase-corrected complex signal at a user-defined spacing $\Delta\rho$ (passed to the `DiffractionLimitedProfile` as the positional argument `dr_km` when instantiating the class). We suggest a value for `dr_km` no smaller than 0.05 km.

To satisfy the sampling theorem, the subsequent diffraction reconstruction resolution can only have shortest resolvable wavelengths of Nyquist or higher (i.e., $\geq 2\Delta\rho$). However, the situation is complicated by a variety of definitions of diffraction reconstruction resolution. As MTR86 point out (see Eqs. 10–14), resolution can be defined in terms of the the filter window width $W$ either as the null-to-null width of the main diffraction lobe, or as the equivalent width of the normalized impulse response profile – these definitions differ by a factor of two from each other. Uncertainty in the Fresnel scale can further degrade the effective resolution, as can limitations on the validity of the approximations made to compute the phase of the signal.

In our development of `rss_ringoccs`, we used the MTR86 Eq. 11 definition of effective resolution $\Delta R_W = 2F^2/W$ and the geometrically scaled definition of $F$ given by MTR86 Eq. 6. This is the definition used throughout MTR86 in the analysis of Voyager RSS data, and it matches our results when we apply diffraction reconstruction to the archived PDS Voyager Saturn and Uranus RSS diffraction-limited profiles. We refer to this as the *processing resolution* $\Delta R$ within `rss_ringoccs`.

In contrast to these conventions, Essam Marouf introduced a different definition of resolution in his Cassini reconstructed profiles available on the PDS, based on applying a low-pass filter to the diffraction reconstruction. The relation between $\Delta R_W$ and this new PDS definition of resolution is given by

$$\Delta R_W = 0.75 \Delta R_{\mathrm{PDS}}$$

or

$$\Delta R_{\mathrm{PDS}} = \frac{4}{3}\Delta R_W.$$

Given these two definitions, and a lack of information about the details of the low-pass filter used by Marouf, we faced a choice: should we retain the definition of resolution as derived in MTR86 and apparently used for Voyager RSS results, or should we be consistent with the recent PDS contributions by Marouf? We chose the latter approach, so that our `rss_ringoccs` runs of Cassini RSS observations were consistent with, and could be directly compared to, the PDS results at the same quoted post-reconstruction resolution. The user specifies a desired resolution $\Delta R_{\mathrm{PDS}}$ for the reconstructed profile through the `res` positional argument when instantiating the `DiffractionCorrection` class. The resolution specified by `res` is then scaled within this class to the processing resolution $\Delta R$ by the factor of 0.75 described above.

In our interpretation of the sampling theorem, `rss_ringoccs` requires that $\Delta R_W > 2\Delta\rho$. In terms of the requested diffraction-corrected resolution $\Delta R_{\mathrm{PDS}}$, this places the following restriction on the pre- and post-diffraction reconstructed resolutions:

$$\Delta R_{\mathrm{PDS}} > \frac{8}{3}\Delta\rho.$$

The factor of 8/3 is non-intuitive, but is the best compromise we could find. As specific example, for a DLP file produced at 0.05 km resolution ($\Delta\rho = 0.05$ km), the requested post-diffraction resolution $\Delta R_{\mathrm{PDS}}$ (or `res`) must be no smaller than $8/3 \times 0.05 = 0.133$ km. (This is below the useful resolution of the majority of Cassini RSS ring observations.) If the user violates these conditions, an informative error message will be displayed, made more comprehensible (we hope!) by this discussion.

# 4    A detailed look at `rss_ringoccs`

Here, we elaborate on the inner workings of `rss_ringoccs`, describing the methods and goals of each step of the software pipeline. For documentation and definition of individual variables, functions, methods, and modules, we refer the user to our online reference available at https://rss-ringoccs.readthedocs.io/en/master/.

## 4.1    RSR reader

The `rsr_reader/` subpackage is used for extracting information from a given RSR file. The `RSRReader` class, when instantiated with a linked RSR file, extracts the raw complex signal $I$ and $Q$ from the RSR file from the PDS as well as some accompanying non-geometric meta-data stored in the RSR file header such as the DSN station, observation dates, sampling rate, start and end times of the observation, and the band of observation.

## 4.2    Occultation geometry routines

The routines in `occgeo/` depend heavily on the NAIF SPICE Toolkit and are geared towards reproducing all occultation geometry parameters that are documented within `Archived_Cassini_RSS_RingOccs_2018`, or `CORSS_8001 v2`, submission (see Table 5). In addition to these parameters, `Geometry` also calculates the optical depth enhancement factor $\beta$ and the effective ring opening angle $B_{eff}$. (See the documentation in the source code `rss_ringoccs/occgeo/calc_occ_geometry.py` for the definitions of these quantities.)

Using orbital parameters compiled from literature and the computed ring azimuth and ring radius, `Geometry` uses the `find_gaps` method from the `cal_occ_geo` module to determine the locations of gaps in the ring system in the occultation data set. This is done iteratively by repeating the following steps, choosing the semimajor axis of the gap edge for the initial predicted edge radius:

1. Find the ring radius in the occultation data set closest to the predicted gap edge radius.

2. Find the ring azimuth and orbital time implied by the closest ring radius.

3. Predict the radius of the gap edges using compiled orbital properties and the implied ring azimuth and time.

| Symbol | Parameter Name | `Geometry` Attribute |
|---|---|---|
| $t_{OET}$ | OBSERVED EVENT TIME | t_oet_spm_vals |
| $t_{RET}$ | RING EVENT TIME | t_ret_spm_vals |
| $t_{SET}$ | SPACECRAFT EVENT TIME | t_set_spm_vals |
| $\rho$ | RING RADIUS | rho_km_vals |
| $\phi_{RL}$ | RING LONGITUDE | phi_rl_deg_vals |
| $\phi_{ORA}$ | OBSERVED RING AZIMUTH | phi_ora_deg_vals |
| $B$ | OBSERVED RING ELEVATION | B_deg_vals |
| $D$ | SPACECRAFT TO RING INTERCEPT DISTANCE | D_km_vals |
| $V_{rad}$ | RING INTERCEPT RADIAL VELOCITY | rho_dot_kms_vals |
| $V_{az}$ | RING INTERCEPT AZIMUTHAL VELOCITY | phi_rl_dot_kms_vals |
| $F$ | FRESNEL SCALE | F_km_vals |
| $R_{imp}$ | IMPACT RADIUS | R_imp_km_vals |
| $r_x$ | SPACECRAFT POSITION X | rx_km_vals |
| $r_y$ | SPACECRAFT POSITION Y | ry_km_vals |
| $r_z$ | SPACECRAFT POSITIION Z | rz_km_vals |
| $v_x$ | SPACECRAFT VELOCITY X | vx_kms_vals |
| $v_y$ | SPACECRAFT VELOCITY Y | vy_kms_vals |
| $v_z$ | SPACECRAFT VELOCITY Z | vz_kms_vals |
| $\theta_{EL}$ | OBSERVED SPACECRAFT ELEVATION | elev_deg_vals |

Table 5: Glossary of parameters in *GEO.TAB file in PDS submission `Cassini_RSS_Ring_Profiles_2018_Archive` and their corresponding attribute names within the `Geometry` class.

This iterative process returns the gap edge radius once it converges to a solution (i.e., when the difference between two consecutive radius predictions is less than one meter) which occurs within five iterations or less. The inner and outer edges of each gap are then stored as an attribute of the `Geometry` object instance for future use.

To create an instance of `Geometry`, or `geo_inst`, users will need an instance of the `RSRReader` class (`rsr_inst`), a target planet, a target spacecraft, a set of kernels over the duration of the RSR file used in `rsr_inst`, and, optionally, a desired number of points per seconds for all calculations (the default is 1 point per second). For choosing an RSR file, which is the only input necessary for instantiating `RSRReader`, see Section 7.2.

## 4.3   Calibration routines

All of the routines needed to produce a calibrated diffraction pattern are in the `calibration/` directory in the `rss_ringoccs` package. Each of them performs a portion of the frequency and power calibration steps. Every step of the calibration process is handled by the `Calibration` class. When instantiated (which requires the appropriate instances of the `RSRReader` and `Geometry` classes), it calls the `FreqOffsetFit` class to compute the offset frequency needed for phase-correcting the measured complex signal. Then, the signal is phase-corrected using the `Calibration` class method `correct_IQ` following Marouf et al. (1986) and Asmar et al. (2018). The phase detrending function $\psi$ is computed from the cumulative integral:

$$\psi = \int^{t} \hat{f}(\tau)_{offset} \, \mathrm{d}\tau + \psi(t_0) \tag{6}$$

and used for detrending the complex signal such that:

$$I_c + iQ_c = [I_m + iQ_m] \exp(-i\psi) \tag{7}$$

(Asmar et al. 2018, Equations 17 and 18). Then, `Calibration` normalizes the phase-corrected signal, using the `Normalization` class to estimate the intrinsic spacecraft power $\hat{P}_0$ as it changes over the course of the occultation.[7] Finally, all the results of the calibration are written out to an `LBL` and a `TAB` file following the naming conventions discussed above.

### 4.3.1 Frequency offset

To estimate the offset frequency over the entire occultation, we compute the offset frequency $f(t)_{offset}$ directly from the raw data using a series of "rolling-window" FFTs. This is stored as an attribute of the `FreqOffsetFit` class for use by the phase detrending method in the `Calibration` class. Beginning with V1.2 of `rss_ringoccs`, `FreqOffsetFit` deviates from previous approaches to fitting the frequency offset residual for several reasons:

1. Some RSR files contain NANs in the file headers in place of the coefficients needed for calculating the polynomials that describe the predicted sky frequency, which prevented computing the residual frequency offset.

2. Computing the predicted sky frequency over the entire occultation added at least 5 seconds of computation time to each of the 151 RSR files at 1 kHz prior to USO failure.

3. Primarily for post-USO failure observations, disagreements between the predicted and reconstructed sky frequency sometimes exceeded 2 MHz and introduced scalloping into the frequency offset, which prevented appropriate description of the frequency offset.

4. Systemically, there is essentially no difference between fitting the frequency offset and the residual frequency offset.

Our new approach not only simplifies the pipeline but also enables support for processing many more files than previously possible.

When instantiated, the `FreqOffsetFit` class begins by instancing the `calc_freq_offset` class, which contains methods to calculate the frequency offset as a function of time from the raw data. It uses the time (`spm_vals`) and raw signal $I_m + iQ_m$ (`IQ_m`) attributes of RSRReader class (`rsr_inst`). Its positional arguments are an instance of the RSRReader class (`rsr_inst`) and two floats specifying the minimum and maximum seconds past midnight (SPM) values to use as limits on the range of occultation data for which the offset frequency is computed (this reduces computation time by eliminating the calculation of offset frequencies that are not useful for constraining the signal offset frequency). Its optional inputs are `dt_freq` for the FFT window size in seconds from which to calculate frequency offset (default is 2 seconds) and `verbose` for a Boolean specifying whether to print out intermediate steps to the terminal (default is `False`).

---

[7]Limits on the reliability of the normalized power are estimated in the form of threshold optical depth, which is computed by the `calc_tau_thres` class when instantiating `DiffractionLimitedProfile()`.

To calculate the frequency offset from the data, we use the `numpy` FFT module to compute the frequency components of the raw measured complex signal for a window in time with a width of `dt_freq` and centered on time `spm_mid`. The submodule `calc_freq_offset` estimates the frequency corresponding to the peak in the power spectrum near the center of the bandpass in two steps. First, it takes a discrete approach by applying a Hamming filter to the signal within the window, computing the discrete FFT, and obtaining the frequency associated with the maximum power ($|A^2|/N$). Second, to better constrain the frequency offset, `calc_freq_offset` takes a continuous approach, computing the continuous Fourier transform of the Hamming-filtered complex signal at a 0.001 Hz sampling in frequency over a 0.5 Hz window centered on the peak frequency found in the discrete Fourier transform. The frequency associated with the maximum power ($|A^2|/N$) of the continuous Fourier transform is taken to be the carrier frequency offset associated with the time `spm_mid`. The result is stored in an array. Then, the window center is shifted forward in SPM by the sampling resolution value, and the process is repeated. The first window is centered at the initial SPM value plus half with window width and is sampled at the keyword-specified resolution until the window center is half a window width from the end of the time series.

| Symbol | Parameter Name | `Calibration` Attribute |
|---|---|---|
| $t_{OET}$ | OBSERVED EVENT TIME | t_oet_spm_vals |
| $\hat{f}(t)_{sky}$ | SKY FREQUENCY | f_sky_hz_vals |
| $\hat{f}(t)_{offset}$ | OFFSET FREQUENCY | f_offset_fit_vals |
| $\hat{P}_0$ | FREESPACE POWER | p_free_vals |

Table 6: Glossary of calibration data in the CAL files.

The `FreqOffsetFit` class then calls `calc_f_sky_recon`, a pythonized version of Nicole Rappaport's PREDICTS Fortran software, to compute the reconstructed sky frequency. This uses spacecraft ephemerides available in the kernel files and `spiceypy` to determine the implied line-of-sight Doppler shift of the intrinsic USO frequency due to the motion of the spacecraft relative to the observing station. This gives a reconstructed sky frequency, denoted as $f(t)_{dr}$.

With its method `create_mask`, `FreqOffsetFit` performs sigma clipping of the offset frequency to exclude unreliable data by creating a boolean mask array. The method begins by masking out all offset frequencies more than five standard deviations away from the median frequency offset.

In order to exclude spuriously included data, `create_mask` performs "nearest-neighbor" comparisons. The first comparison examines the four nearest data points included by the boolean mask. If the absolute difference between the considered datum and each of its four neighbors exceeds 0.25 Hz, the datum is excluded. The second comparison assumes any datum with at least four excluded nearby data points should also be excluded. Finally, a boolean mask array is returned that excludes all unreliable data.

`FreqOffsetFit` uses its `fit_f_sky_offset` method to fit a polynomial (of order specified by the `calc_polyorder` method to prevent over-fitting) to the masked frequency offset

data using the `numpy.polynomial` subpackage. This method fits data with polynomials of iteratively increasing order, using the F-test statistic to evaluate whether a higher order polynomial provides a statistically significantly better fit to the frequency offset data. The method stops when increasing the polynomial order does not provide a better description or when the polynomial order exceeds nine. The best-fit polynomial $\hat{f}(t)_{offset}$ is returned along with the reduced summed squared residuals as an estimate of the fit quality.

If the occultation occurred after the failure of the on-board USO, then before fitting the polynomial, `FreqOffsetFit` calls its `find_disconts` method to look for discontinuities in the frequency offset. This uses the central finite difference method to compute the second-order derivative of the masked frequency offset, accounting for non-uniform sampling introduced by the sigma clipping. Then, `find_disconts` computes the local maxima in the second derivative to determine where large changes in slope have occurred. To determine if a change in slope is associated with a discontinuity, `find_disconts` checks several cases: (i) to exclude variations due to noise, the absolute difference in masked frequency offset values about each maximum must vary by more than 0.05 Hz; (ii) to prevent falsely identifying the gap in frequency offset introduced by the B ring as discontinuity, the maximum must not occur within the B ring; (iii) to prevent any gaps in the data from being flagged as discontinuities, the difference in SPM between masked frequency offsets about the mamximum must not exceed 10,000 seconds; (iv) to prevent issues with frequency offset fitting, the number of data between any two maxima or any maximum and an end point must exceed 10. All maxima in the second order derivative satisfying these criteria are returned to `FreqOffsetFit`. Finally, `FreqOffsetFit` defines segments based on the end points of the masked frequency offset and the returned maxima. `FreqOffsetFit` fits each with a polynomial of order determined by `calc_polyorder` for that segment, with a maximum polynomial order of 4. While this adds support for calibration of several post-USO occultations, some improvements must be made to the discontinuity-finding method in the future to extend support to the total post-USO data set.

`FreqOffsetFit` computes $\hat{f}(t)_{offset}$ and stores both the $\hat{f}(t)_{dr}$ and $\hat{f}(t)_{offset}$ variables as attributes. For reference and visual assessment, `FreqOffsetFit` plots the total and sigma-clipped sets of $f(t)_{offset}$ and overplots $\hat{f}(t)_{offset}$. The plot is saved in the appropriate output directory and is named following the `*.TAB` and `*.LBL` conventions with the infix `FORFIT`.

### 4.3.2 Power normalization

After phase compensation of the complex signal, the `Calibration` class instantiates the `Normalization` class. The objective of this class is to estimate the intrinsic spacecraft signal power $\hat{P}_0$ by fitting the observed power in free space regions with a low-order polynomial. A `Normalization` instance requires $I_c + iQ_c$ and an instance of the `Geometry` class (`geo_inst` in the pipeline scripts).

To begin, `Normalization` down-samples the corrected complex signal by a factor of 500. This serves to minimize the effect of extended ring diffraction patterns in the free space regions on the overall prediction of $\hat{P}_0$ while expediting the fitting procedure.

Next, `Normalization` utilizes the ring gaps and other free space regions predicted by the `find_gaps` function in the `calc_occ_geo` submodule in units of SPM. Free space regions are then excluded or retained by comparing the median power within the SPM limits of the free space region to the maximum power *within* the ring system. Because extinction by the ring material causes a decrease in observed signal power, this effectively selects the maximum power observed in gaps and divisions inside of the ring system. When the median power within a given free space region is 50% below or 25% above the maximum ring-system spacecraft signal power, the data from this free space region are excluded. After these comparisons and rejections are made, data from all remaining free space regions are assembled for use in a polynomial fit.

The `Normalization` method `fit_freespace_power` then fits these reliable measurements of the intrinsic spacecraft signal in order to estimate $\hat{P}_0$ over the entire occultation. The default fit is a third order polynomial; however, the fit order can be changed when instantiating the `Calibration` class using the keyword argument `pnf_order` and the fit type can be set using the keyword argument `pnf_fittype` (default of "poly" for polynomial and "spline" for spline, piece-wise is on lien for future versions). Regardless of user input, if the number of free space regions is less than five, the fitting method forces the fit order to linear.

If the keyword `interact` is set to `True` when instantiating the `Calibration` instance, `Normalization` will enter its interactive mode after computing the best fit to the reliable free space data. In this mode, users can customize the free space regions, fit type, and fit order following prompts in the terminal. The command line will prompt the user to confirm interactive mode and subsequently display a plot in a `matplotlib.pyplot` window showing the best-fit polynomial to the default free space regions. Both the individual regions and the total profile will be displayed so that the user may assess the quality of the fit (in the same manner as the output fit plot, as shown in Figure 15). The command line will then prompt users whether to change included free space regions or revert to the defaults generated by the automated pipeline (see Appendix C for an example). If the user opts to change the free space regions, new definitions for the desired free space regions (specified as pairs of lower and upper SPM limits for each region) will need to be entered in the following format

$$[[30500,31785],[34080,34245],[35285,36000]]$$

to be used in the fit. If the new free space region limits are not entered in the appropriate format, the code will revert to the initial freespace regions predicted by `Geometry`.

Once the final fit has been computed, $\hat{P}_0$ and the boundaries of the free space regions used to compute the fit are stored as attributes. As with the frequency offset fit, this step also includes plotting the fit results for visual inspection and reference. $\hat{P}_0$ is plotted over the phase-compensated signal power for both the entire profile and for each individual free space region used in the fit. Naming convention follows that of the `*.TAB` and `*.LBL` files with the infix `FSPFIT`.

## 4.4 Diffraction-limited profile routines

| Symbol | Parameter Name | `NormDiff` Attribute |
|---|---|---|
| $\rho$ | RING RADIUS | rho_km_vals |
| $\Delta\rho_{IP}$ | RADIUS CORRECTION DUE TO IMPROVED POLE | rho_corr_pole_km_vals |
| $\Delta\rho_{TO}$ | RADIUS CORRECTION DUE TO TIMING OFFSET | rho_corr_timing_km_vals |
| $\phi_{RL}$ | RING LONGITUDE | phi_rl_rad_vals |
| $\phi_{ORA}$ | OBSERVED RING AZIMUTH | phi_ora_rad_vals |
| $\tau$ | NORMAL OPTICAL DEPTH | tau_norm_vals |
| $\phi$ | PHASE SHIFT | phase_rad_vals |
| $\tau_{TH}$ | NORMAL OPTICAL DEPTH THRESHOLD | tau_threshold_vals |
| $t_{OET}$ | OBSERVED EVENT TIME | t_oet_spm_vals |
| $t_{RET}$ | RING EVENT TIME | t_ret_spm_vals |
| $t_{SET}$ | SPACECRAFT EVENT TIME | t_set_spm_vals |
| $B$ | OBSERVED RING ELEVATION | B_rad_vals |

Table 7: Glossary of optical depth, phase shift, and selected geometry parameters contained in the DLP files.

When instantiated, the `DiffractionLimitedProfile` class normalizes the power profile using the results from the `Calibration` step and resamples it with respect to uniformly-spaced ring radius at a sample spacing $\Delta\rho$. The `DiffractionLimitedProfile` class requires all previous class instances as arguments: the `RSRReader` class (`rsr_inst`), the `Geometry` class (`geo_inst`), and the `Calibration` class (`cal_inst`). The final positional argument `dr_km` specifies the radial sample spacing of the profile. Keyword arguments consist of the `verbose` – a boolean specifying verbose mode (default is `False`), `write_file` – a boolean specifying whether to write the DLP out to a CSV file (default is `True`), and `profile_range` – a $1 \times 2$ list setting the lower and upper limits of the ring plane radial range of the DLP, in km (the default values are `[65000,150000]`, which span Saturn's classical ring system; we strongly recommended that users proceed with these default limits).

When instantiated, the `DiffractionLimitedProfile` calls the `resample_IQ` module to resample the phase-detrended signal $I_c + iQ_c$ with respect to ring radius over the range `profile_range` at radial spacing of `dr_km`. In the event that the user-provided `dr_km` spacing is finer than the average raw radial spacing, the resampling routine will compute the lowest possible sample spacing and resample the complex signal to this spacing instead of `dr_km`. If this occurs, the user will be notified in the command line, and all documentation of the diffraction-limited profile will reflect the sample spacing used rather than the sample spacing specified by `dr_km`.

From the resampled detrended complex signal, `DiffractionLimitedProfile` computes the phase

$$\phi_c = \arctan(Q_c, I_c) \tag{8}$$

and normalized complex signal

$$\hat{T} = \hat{T}_R + i\hat{T}_I = (I_c + iQ_c)/\hat{P}_0, \tag{9}$$

the latter following from Equation 2 in Marouf et al. (1986) and Equation 20 in Asmar et al. (2018). The diffraction-limited DLP normal optical depth $\tau_{DLP}$ is calculated from

$\hat{T}$ using:

$$\tau_{DLP} = -\sin(|B|)\ln(\hat{T}) \tag{10}$$

Finally, `DiffractionLimitedProfile` calls the `calc_tau_thresh` submodule to compute the threshold optical depth $\tau_{TH}$, a proxy for the maximum reliable value of $\tau_{DLP}$.

For the DLP instance to be of use in the subsequent diffraction reconstruction step of the pipeline, $\dot{\rho}$ cannot change sign over the course of an occultation. Chord and proximal orbit occultations thus present a problem if not handled appropriately when creating the DLP object.

`DiffractionLimitedProfile` handles this issue by using a class method to return an object instance of itself for each direction of the occultation as indicated by the sign of $\dot{\rho}$. For the user, this means that instantiating the `DiffractionLimitedProfile` object class will always return two objects: one for ingress and one for egress (always in this order). For diametric occultations, the object corresponding to the direction *not* included in the observation will be a `None` object in place of a DLP instance. For chord occultations, the user will receive two DLP object instances, one for ingress and one for egress, split where a sign change in $\dot{\rho}$ occurs. Each DLP object can be passed individually to the diffraction reconstruction step in the pipeline.

### 4.4.1 Threshold optical depth

The threshold optical depth is an estimate of the maximum reliable value of optical depth implied by the signal-to-noise ratio $\mathrm{SNR}_0$. The noise is estimated from the STFT of the entire observation of raw $I + iQ$. After computing the STFT, we average the power spectrum over the frequency ranges $-450$ to $-200$ Hz and $200$ to $450$ Hz so as to eliminate both the spacecraft carrier signal and the rolloff at the edges of the power spectrum. Then, we average the frequency-averaged power over the first and last thousand seconds of the observation to exclude possible contamination from scattered spacecraft signal while maintaining a large number of samples of the noise. The intrinsic signal $\hat{P}_0$ is assumed to be the fit to the freespace regions computed in the calibration step and stored as an attribute of the `DiffractionLimitedProfile` class. We consider the ratio of $\hat{P}_0$ and the average noise to be $\mathrm{SNR}_0$.

Following Equations 24-26 in Marouf et al. (1986) and Equations 26 and 27 in Asmar et al. (2018), we compute the threshold optical depth using

$$\tau_{TH} = -\sin(|B|)\ln\left[\frac{C_\alpha\dot{\rho}}{2\mathrm{SNR}_0\Delta\rho}\right] \tag{11}$$

where $B$ is the ring opening angle and $\dot{\rho}$ is the ring intercept radial velocity as computed by and attributed in the `Geometry` class, $C_\alpha = 2.41$ is chosen to correspond to 70% confidence[8], and $\Delta\rho$ is the radial spacing. For the DLP class, this is simply the `dr_km` positional argument specified when instantiating the DLP class and has a default of 0.25 km. For the reconstructed profile, $\Delta\rho$ will depend on the window size $W$ and Fresnel scale $F$, the so-called *processing resolution* $\Delta R = 2F^2/W$. We show the dependence of

---

[8]From Marouf et al. (1986) Equation 25, this is given by the root-mean-square of the difference between the measured complex signal $X = T + n$ (where $n$ is the additive noise from the receiver) and actual complex signal $T$, normalized with respect to the expected receiver noise $P_N$.
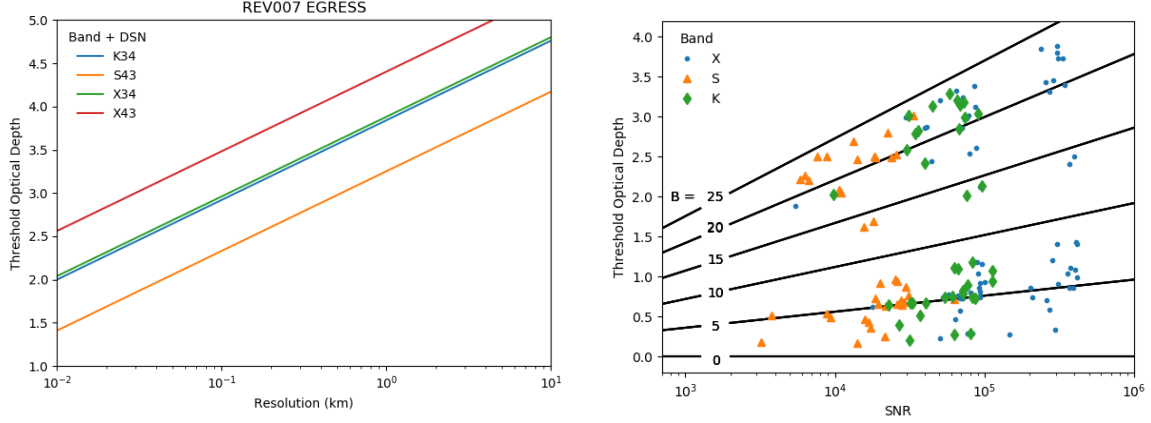
Fig. 6: *Left:* Resolution dependence of $\tau_{TH}$ for Rev 007 E. *Right:* Effect of opening angle $B$ on $\tau_{TH}$ as a function of $SNR_0$ for $\Delta\rho = 0.25$ km. Data are for all 1 kHz files prior to USO failure

$\tau_{TH}$ on resolution in Figure 6 (cf. Fig. 8, Marouf et al. 1986). Also in Figure 6 is a demonstration of the effects of both opening angle and SNR on $\tau_{TH}$ for all 1 kHz RSR files prior to USO failure.

## 4.5 Diffraction reconstruction routines

| Symbol | Parameter Name | Attribute Name |
|---|---|---|
| $\Delta R$ | RECONSTRUCTION RESOLUTION (KM) | res |
| $\rho$ | RING RADIUS | rho_km_vals |
| $\Delta\rho_{IP}$ | RADIUS CORRECTION DUE TO IMPROVED POLE | rho_corr_pole_km_vals |
| $\Delta\rho_{TO}$ | RADIUS CORRECTION DUE TO TIMING OFFSET | rho_corr_timing_km_vals |
| $\phi_{RL}$ | RING LONGITUDE | phi_rl_rad_vals |
| $\phi_{ORA}$ | OBSERVED RING AZIMUTH | phi_rad_vals |
| $\tau$ | NORMAL OPTICAL DEPTH | tau_vals |
| $\phi$ | PHASE SHIFT | phase_rad_vals |
| $\tau_{TH}$ | NORMAL OPTICAL DEPTH THRESHOLD | tau_threshold_vals |
| $t_{OET}$ | OBSERVED EVENT TIME | t_oet_spm_vals |
| $t_{RET}$ | RING EVENT TIME | t_ret_spm_vals |
| $t_{SET}$ | SPACECRAFT EVENT TIME | t_set_spm_vals |
| $B$ | OBSERVED RING ELEVATION | B_rad_vals |
| $w$ | WINDOW WIDTH FOR RECONSTRUCTION | w_km_vals |
| $f_{sky}$ | SKY FREQUENCY | f_sky_hz_vals |
| $F$ | FRESNEL SCALE | F_km_vals |
| $D$ | SPACECRAFT-RIP DISTANCE | D_km_vals |
| $\hat{T}$ | DIFFRACTED COMPLEX TRANSMITTANCE | T_hat_vals |
| $T$ | RECONSTRUCTED COMPLEX TRANSMITTANCE | T_vals |

Table 8: Glossary of parameters contained in RSS_2005_123_X43_E_TAU_01KM.TAB. See companion label (.LBL) files for description of the data.

All of the diffraction reconstruction tools are located within the `diffrec` subpackage of `rss_ringoccs`. We include simple tools for diffraction reconstruction of the diffraction pattern contained in an instance of the `NormDiff` class, as well as more complex tools for modeling problems and comparing them with real-world data and geometry. The main

dependency is the `numpy` package, but some functions also rely on tools found in the `scipy` package. The subpackage is broken into four submodules:

- `advanced_tools`
- `diffraction_correction`
- `special_functions`
- `window_functions`

The `diffraction_correction` submodule is the primary tool within `diffrec` and contains the `DiffractionCorrection` class, which is the main utility for creating diffraction-reconstructed profiles of radio occultation observations. The Python syntax is as follows:

```
In [1]: from rss_ringoccs import diffrec
In [2]: rec = diffrec.DiffractionCorrection(norm_inst, res)
```

Here, `norm_inst` is an instance of the `DiffractionLimitedProfile` class containing the diffracted data and `res` is the user-requested processing resolution of the reconstructed profiles in kilometers and expressed as a floating point number. There are several keywords in this class to allow the user to specify how the diffraction reconstruction will be performed.

A new feature of `rss_ringoccs` is the use of special polynomials within the diffraction reconstruction steps to greatly reduce computation time without sacrificing accuracy. The *Fresnel kernel*, $\psi(\rho, \rho_0; \phi, \phi_0)$, needs to be computed at its *stationary* value, $\psi_s$:

$$\frac{\partial \psi_s}{\partial \phi} = 0. \tag{12}$$

We expand $\psi$ in a Taylor expansion about the point $\phi_0$, and obtain the following:

$$\psi = \sum_{n=0}^{\infty} \psi^{(n)}(\rho, \rho_0; \phi_0, \phi_0) \frac{(\phi - \phi_0)^n}{n!}. \tag{13}$$

The notation $\psi^{(n)}$ represents the $n^{\text{th}}$ partial derivative of $\psi$ with respect to $\phi$. The tuple $(\rho, \rho_0; \phi_0, \phi_0)$ is to indicate that the coefficients of the Taylor expansion are *functions of the other variables*, and are not constants. We apply Newton-Raphson to find the stationary value of $\psi$, and obtain in the first perturbation the following value:

$$\phi_s = \phi_0 - \frac{\psi'(\rho, \rho_0; \phi_0, \phi_0)}{\psi''(\rho, \rho_0; \phi_0, \phi_0)}, \tag{14}$$

where, again, derivatives are taken with respect to $\phi$. Truncating Eq. 13 at the quadratic term and evaluating at $\phi = \phi_s$, we obtain:

$$\psi_s \approx \psi(\rho, \rho_0; \phi_0, \phi_0) - \frac{1}{2} \frac{\psi'(\rho, \rho_0; \phi_0, \phi_0)^2}{\psi''(\rho, \rho_0; \phi_0, \phi_0)}. \tag{15}$$

The nature of $\psi$ allows the right-hand side of Eq. 15 to be expressed exactly in terms of Legendre polynomials. For example, stopping the Legendre expansion at the quadratic term gives the classic *Fresnel approximation*. This is:

$$\psi_s = \frac{\pi}{2} \left( \frac{\rho - \rho_0}{F} \right)^2. \tag{16}$$

We will refer to this approach to the expanson as Fresnel-Legendre polynomials. `rss_ringoccs` allows for several different polynomial powers of this expansion by using the `psitype` keyword. This is a `string`, and the following inputs are allowed:

- 'Fresnel' - Classic Fresnel approximation.

- 'Fresnel3' - Legendre expansion up to the cubic term.

- 'Fresnel4' - Legendre expansion up to the quartic term.

- 'Fresnel6' - Legendre expansion up to 6th order.

- 'Fresnel8' - Legendre expansion up to eighth order.

- 'Full' - No approximation, Newton-Raphson is applied.

For all but Rev133, the 'Fresnel4' option is more than adequate, and can reproduce the PDS results, as well as mimic the results obtained by using 'Full'. Unless overruled explicitly by the user, 'Fresnel4' is the default option. For Rev 133 observations, when the rings were observed nearly edge-on, a known problem with the cubic term of $\psi$ persists, and the Fresnel-Legendre polynomials cannot adequately capture this. This is in part because the Fresnel-Legendre expansion assumes that the first iterate of the Newton-Raphson approximation is sufficient, whereas in such extreme geometries it is not.

Below is a detailed description of the example included in the `quick_look_run.py` script discussed in Section 3.4. As with the quick-look script itself, this example assumes that the user has available the requisite `*.TAB` files generated by the example end-to-end script covered in Section 3.3. The `ExtractCSVData` class covered in the next section can be used to extract information from the `*.TAB` files and reconstruct the DLP instance `norm_inst`.

```
In [1]: geo = "../Data/GEO.TAB"
In [2]: cal = "../Data/CAL.TAB"
In [3]: dlp = "../Data/DLP.TAB"
In [4]: from rss_ringoccs.tools import ExtractCSVData
In [5]: from rss_ringoccs import diffrec
In [6]: norm_inst = ExtractCSVData(geo, cal, dlp, verbose=False)
In [7]: tau_inst_f = diffrec.DiffractionCorrection(
   ...: norm_inst, 1.0, rng="all", psitype="fresnel")
Computation Time: 12.491324
```

Note the quite short (12 second) reconstruction time, due in part to the 'Fresnel' setting for psitype and 1 km resolution. Running `DiffractionCorrection` with psitype='full':

```
In [8]: tau_inst_v = diffrec.DiffractionCorrection(
   data, 1.0, psitype="full", verbose=True)
   Things print out here...
Computation Time: 108.427886
In [9]: tau_inst = diffrec.DiffractionCorrection(
   data, 1.0, psitype="full")
Computation Time: 76.470007
```

There are several things to note here. The computation of $\psi$ is one of the slowest parts in the entire diffraction reconstruction algorithm. In particular, the computation of the

*stationary phase* can be quite time-consuming. Since 'Fresnel' skips all of this, we see a substantial reduction in computation time. The data set that was used in this example comes from the Cassini rev007E occultation observation. We can check the validity of Fresnel approximation for this set by looking at the difference in the two reconstructions. Note that since the power is normalized to 1, this is both fractional and absolute error:

```
In [10]: import numpy as np
In [11]: np.max(np.abs(recf.power_vals-rec.power_vals))
Out[11]: 0.00016784579326811766
In [12]: np.mean(np.abs(recf.power_vals-rec.power_vals))
Out[12]: 3.5374768401331293e-06
```

The Fresnel approximation works very well here. The default setting of psitype='Fresnel4' is slightly slower than 'Fresnel', but still finishes execution in less than 20 seconds. For many occultations where 'Fresnel' fails, 'Fresnel4' still produces accurate results. Another thing to note is that there is a large discrepancy in the computation time for when verbose=True and verbose=False is set. Since verbose prints out pieces of information for every point that is being reconstructed, the Python interpreter needs to wait for the line to be printed before it can process the next point. In most cases this is not an issue, but when speed is crucial it may be better to leave verbose set to False.

## 4.6   Utility routines

Within the `tools/` subpackage one can find various `pds3_*_series.py` scripts and routines to read and write PDS3-type data and label files.[9]  `rss_ringoccs` manages the file naming conventions and calling of the `pds3_*_series.py` scripts by means of the `write_output_files.py` script.

Also included as a utility for the quick-look pipeline is the `ExtractCSVData`, a tool for extracting information from the `*.TAB` files and reconstructing the DLP instance `norm_inst`. This can be found in the `CSV_tools` submodule of the `tools` subpackage, all contained within `rss_ringoccs`. The steps for importing are shown below.

The `ExtractCSVData` imports user-specified `*.TAB` files produced by the end-to-end pipeline and uses them to construct an instance of the `NormDiff` class that can then be passed on for diffraction reconstruction as a part of the quick-look process. This way, the pipeline only needs to be run once on a given data set, and then the user may experiment with different resolutions, window functions, etc., on the diffracted data without repeated time consuming steps. For example, from the master directory of `rss_ringoccs`, one could use ipython to implement the following to construct a `DiffractionLimitedProfile` instance from `*.TAB` files output from a previous run:

---

[9]The products of these routines have not been thoroughly checked for PDS3 compliance.

```
cd ~/Research/rss_ringoccs-master
ipython
In [1]: path ='../output/Rev007/E/Rev007E_RSS_2005_123_X43_E/'
In [2]: geo = path+'RSS_2005_123_X43_E_GEO_20180926_0001.TAB'
In [3]: cal = path+'RSS_2005_123_X43_E_CAL_20180926_0001.TAB'
In [4]: dlp = path+'RSS_2005_123_X43_E_DLP_0100M_20180926_0001.TAB'
In [5]: from rss_ringoccs.tools.CSV_tools import ExtractCSVData
In [6]: from rss_ringoccs import diffrec
In [7]: dlp_inst = ExtractCSVData(geo, cal, dlp, verbose=True)
Extracting Data from CSV Files:
    Extracting Geo Data...
    Geo Data Complete.
    Extracting Cal Data...
    Cal Data Complete.
    Extracting DLP Data...
    DLP Data Complete
    Retrieving Variables...
    Computing Variables...
    Interpolating Data...
    Data Extraction Complete.
    Writing History...
    History Complete.
    Extract CSV Data Complete.
```

Also note that it is possible to combine `*.TAB` files from different end-to-end runs of `rss_ringoccs`, which is encouraged for users who want to examine the effect different calibration inputs might have on the final reconstructed optical depth profile.

The `CompareTau` tool, found in the `advanced_tools` submodule of the `diffrec` subpackage, imports user-specified `*.TAB` files produced by the end-to-end pipeline and runs the diffraction reconstruction at an additional user-specified spatial resolution for the purpose of comparing optical depth profiles for the same occultation with the only difference being the processing resolution.

### 4.6.1 PDS3Reader

The `PDS3Reader` function allows users to easily read in a set of PDS3-formatted data and label files without having to scroll through and examine a label file in detail (for column headers, etc.). To use this function, first verify that the desired data and label file are within the same directory. Then, follow the example below but replace `lbl_file` with the path to the desired label file.

```
ln [1]: import rss_ringoccs as rss
ln [2]: lbl_file = 'RSS_2005_123_X43_E_GEO_20180926_0001.LBL'
ln [3]: geo = rss.tools.PDS3Reader(lbl_file, use_attr_names=False)
```

The `geo` variable will contain two classes as attributes: `series` and `keywords`. `series` refers to the actual data set, and calling `geo.series.__dict__.keys()` will print all the data column headers, as seen in the label file. By setting the keyword argument `use_attr_names` to `True`, these column header names will be replaced by the attribute name used in `rss_ringoccs` to represent the same variable (see Tables 5-7). To grab the data associated with the column header, simply call `geo.series.XX`, where `XX` is the header name. `keywords` contains all of the keywords listed in the label file, and the corresponding keyword values can be called in a similar fashion: `geo.keywords.XX`,

where `XX` is the keyword name. Definitions for these keywords can be found in the online PDS data dictionary https://pds.nasa.gov/tools/dd-search/.

### 4.6.2  Label history

Each label file produced by `rss_ringoccs` contains a `PROCESSING_HISTORY_TEXT` that lists user information (such as Python version, operating system, etc.) as well as an accumulated list of all positional and keyword arguments that were used to run the pipeline up to part where the label was created. Users can visually read this list and rerun the pipeline to reconstruct the same profile. Alternatively, users can use the `read_history` function, which will automatically read in the listed inputs and output a requested instance, if available. For example, a *TAU.LBL file will contain all of the inputs to the `RSRReader`, `Geometry`, `Calibration`, `DiffractionLimitedProfile`, and `DiffractionCorrection` classes. Using `read_history` on the *TAU.LBL will give users the option of returning an instance of any of the above classes.

This function is useful in particular for those who wish to produce a `dlp_inst` sampled at finer radial intervals than that in the original DLP file.

### 4.6.3  Science tools

Some preliminary modeling tools are provided here for use with the data products from `rss_ringoccs`. The script `dtau_miescatt_partsize_grid.py` is one such tool. This script can be run from anywhere in the software directory structure and has no dependencies on other `rss_ringoccs` scripts. However, this tool does require the use of an external package, `PyMieScatt`, which can readily be installed using `pip` as shown here:

```
pip install pymiescatt
```

Following Marouf et al. (1983), this script calculates predictions for observed differential optical depth assuming a power law distribution of particle sizes. Users can specify the ring material index of refraction, range of particle sizes, and power law indices by editing the preamble in the script file. Running the script will output a CSV file and plot, both containing the differential optical depths predicted by Mie scattering physics for the given index of refraction, particle sizes and distributions. These predictions are intended for comparison with differential optical depths calculated from reconstructed normal optical depth profiles output by the `rss_ringoccs` pipeline.

## 4.7  Incoherent signal routines

All of the routines to produce the incoherent signal results are in the `scatter/` directory in the `rss_ringoccs` package. One tool performs the STFT spectrogram calculations and stacking to improve SNR. The other is a tool for users to read in results from the spectrogram output file. The `spectrogram.py` script contains the object class `Scatter`. Instantiating this object requires instances of the RSRReader, Geometry, and Calibration classes. `Scatter` uses the `spectrogram` method from the `scipy.signal` module with a Hamming window to compute the discrete short-time Fourier transform of the phase-corrected complex signal over the entirety of the occultation. Then, its `stack_spec` method stacks the spectrogram slices to boost the SNR of the incoherent signal, which is typically only 1-2 dB above the noise threshold. Following rss_ringoccs file nomenclature,

`Scatter` outputs the spectrogram and ancillary information (e.g., radius, frequency, and time dimensions) to comma-delimited files. We provide the script `spectro_reader.py` as a tool for reading the output spectrogram and ancillary reference files to build the spectrogram, time, frequency, and radius arrays. As a demonstration for reading and visualizing the incoherent signal, we provide an example script `spectrogram_plot_example` in the `examples` directory that reads in scattered signal data products and normal optical depth profiles from the `output` directory and plots the results.

# 5 Validation of `rss_ringoccs` algorithms

In this section, we present tests and validations of the performance and output of `rss_ringoccs`. Perhaps most significantly, this includes a comparison of `rss_ringoccs` results with those published on the PDS as these results were processed using state-of-the-art methods following Marouf et al. (1986). This includes a demonstration of the results for Cassini and for Voyager, results from raw data sampled at different rates, and results from DLPs sampled at different rates.

## 5.1 Comparison with results on the PDS

### 5.1.1 Cassini RSS results

The results of `rss_ringoccs` match those in PDS `CORSS_8001` extremely well. After completing the Huygens ringlet end-to-end example in Section 3.3, several data products will be created. In Figs. 7-8, we compare our output GEO file, plotted in blue, with the PDS GEO file, plotted in dashed red lines. These values are, for our purposes, essentially the same – the comparisons without grey dots indicating a fractional error match exactly to the precision listed in the files.

The calibration steps require more complex calculations and some user judgment, but overall the agreement between the calibrated diffraction-limited profiles obtained from `rss_ringoccs` and the archived PDS results remains excellent. An important calibration step is to normalize the signal power such that it reaches unity within free-space regions, but the fit type and order rely heavily on user choices. For example, although Figure 9 looks as though the signal power outside of the ring system is at unity, indicating a good fit, if we zoom into a feature and compare our final signal power to that on the PDS, the unity background signals differ slightly. For the examples here, this is seen in the Maxwell ringlet but not the Huygens ringlet.
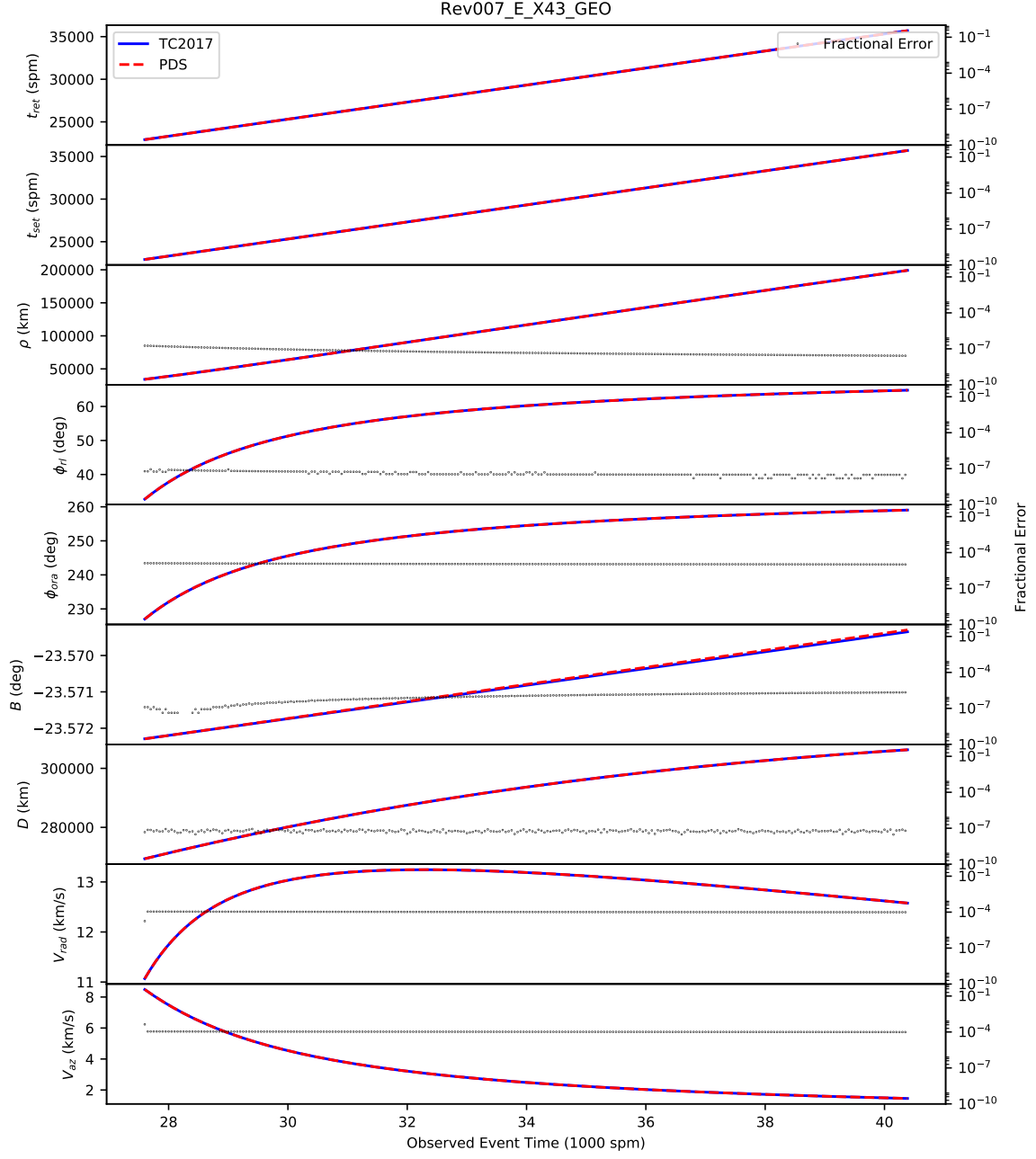
Fig. 7: Comparison of geometry parameters for Rev007 Egress X-band as viewed from DSS-43. PDS `CORSS_8001` data product `Rev007/Rev007E/Rev007E_RSS_2005_123_X43_E/RSS_2005_123_X43_E_GEO.TAB` values are plotted in dashed red lines, with `rss_ringoccs` values overplotted in blue. Fractional error between the two are plotted on the right-hand y-axis in grey dots.
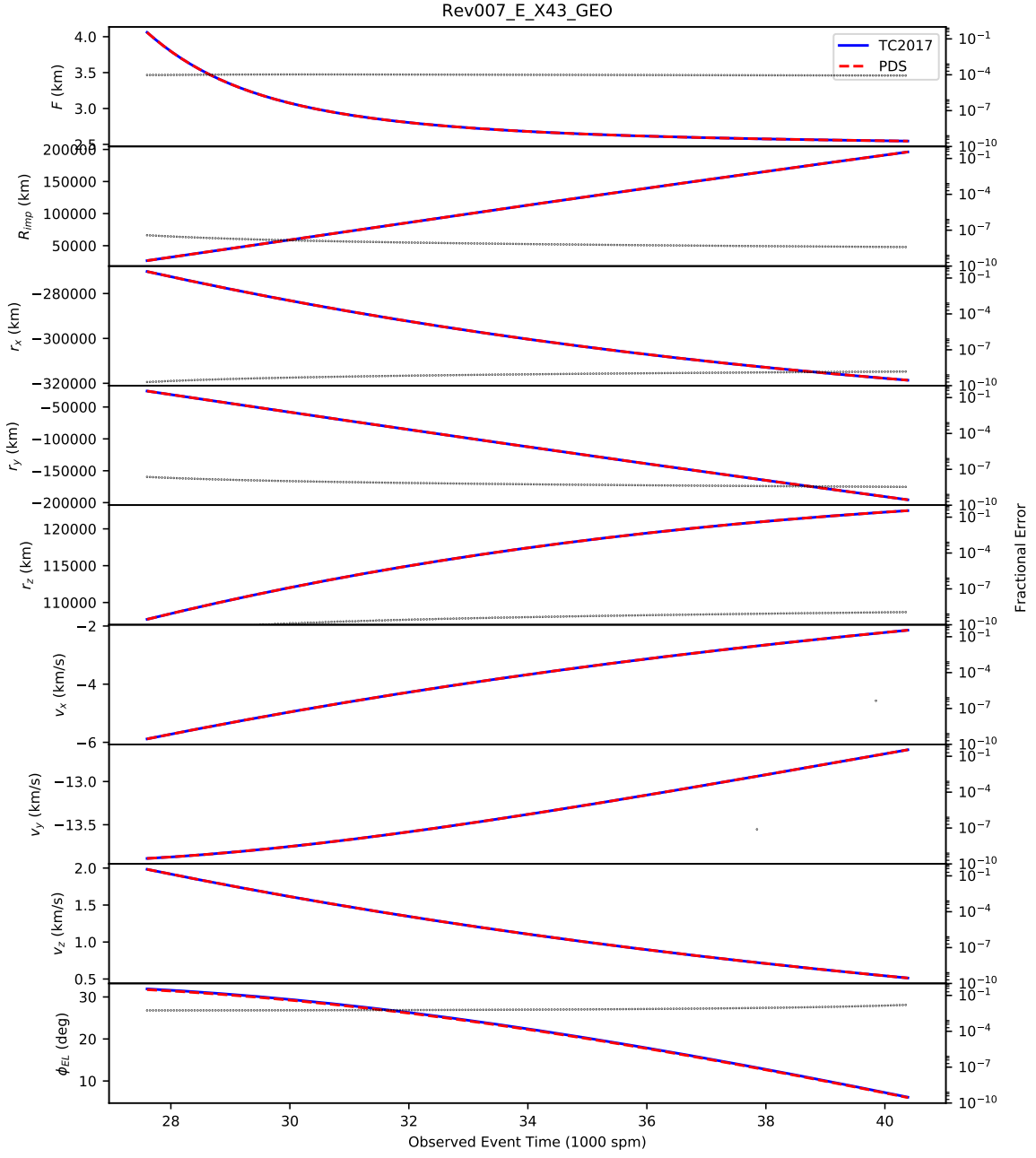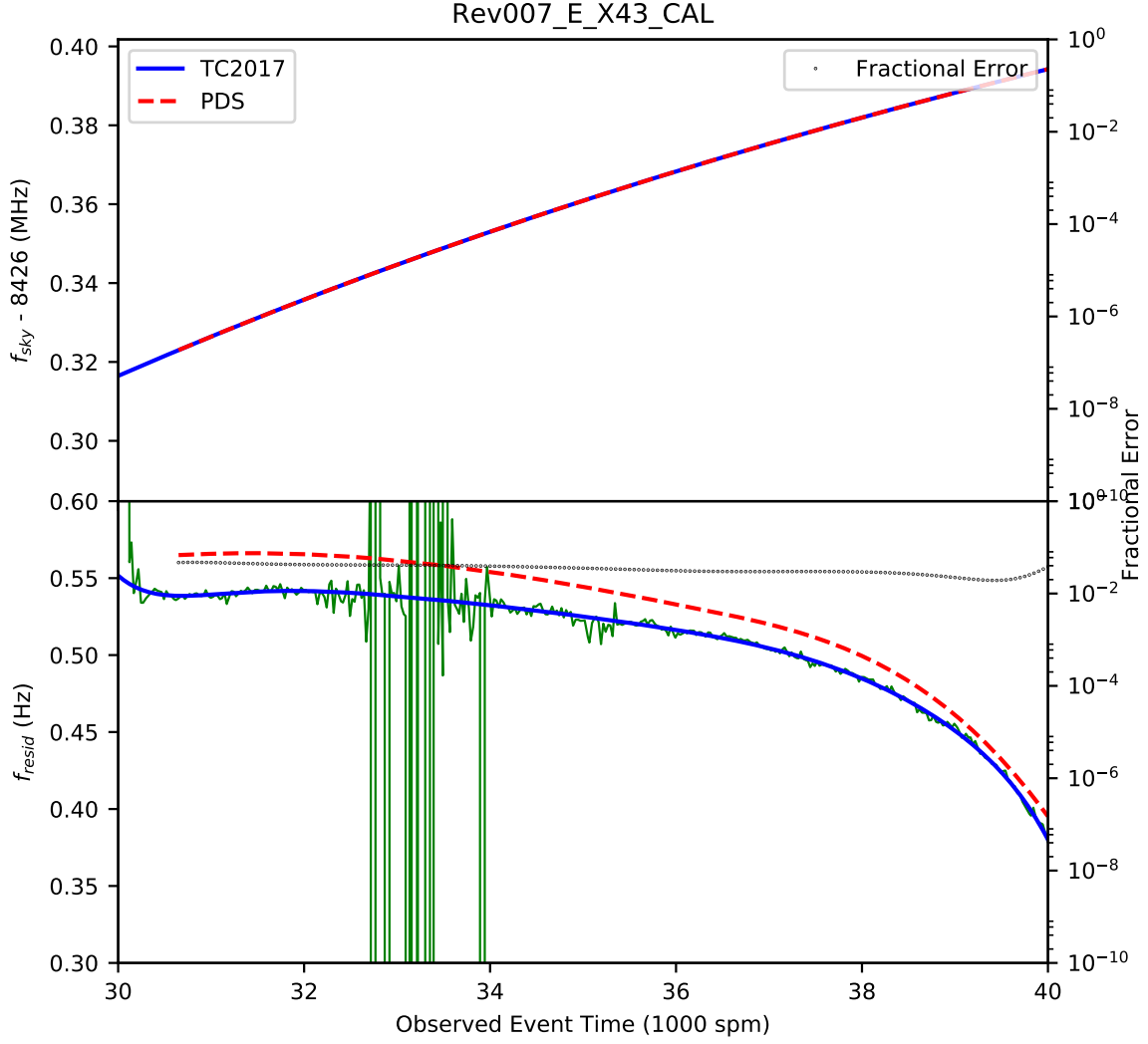
Fig. 8: Comparison of geometry parameters for Rev007 Egress X-band as viewed from DSS-43. PDS `CORSS_8001` data product `Rev007/Rev007E/Rev007E_RSS_2005_123_X43_E/RSS_2005_123_X43_E_GEO.TAB` values are plotted in dashed red lines, with `rss_ringoccs` values overplotted in blue. Fractional error between the two are plotted on the right-hand y-axis in grey dots.

Fig. 9: Comparison of the Frequency Offset and Residual Frequency computed for the Rev007 E X43 data set.

If Fig. 9 we plot the output of the calibration steps of the pipeline for the Rev007 E X43 data set. Plotted with this are the results found on the PDS, as well as the fractional error between the two. Below in Fig. 10 we plot the raw power that is extracted from the RSR files:
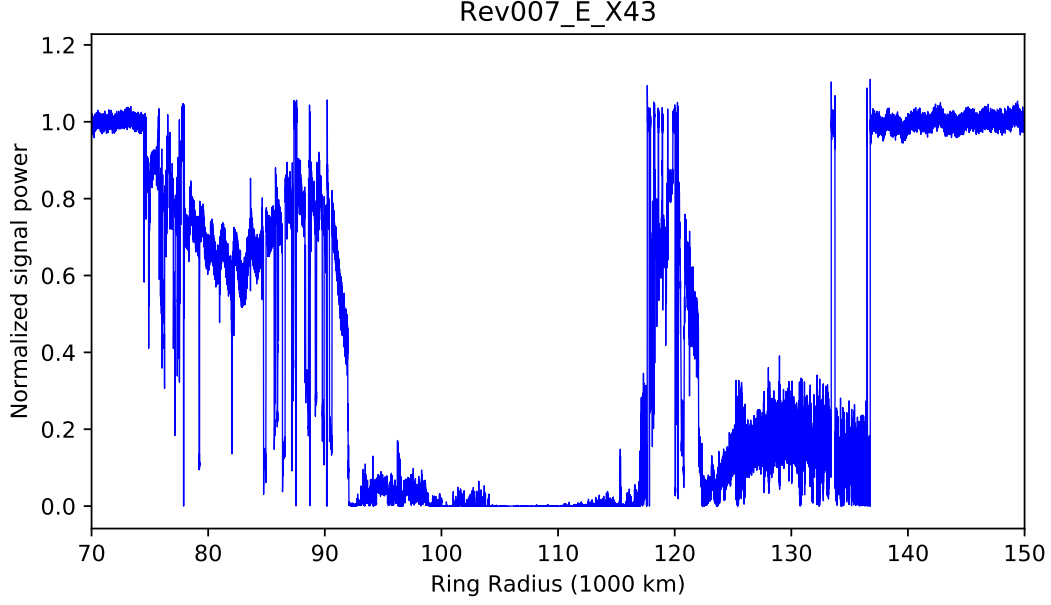
Fig. 10: Raw Power from Rev007 E X43

Finally, at the end of the pipeline we obtain the reconstructed profiles of the Saturnian ring system. It is important to note that the normalization step can be very subtle. As an example of this, we show the reconstruction of Rev007 E X43 in Fig 11 about the Huygens ringlet and the Maxwell ringlet. The default fit was used to create the normalized power. The fit and reconstruction worked extremely well for Huygens, but there is a slight discrepancy for the Maxwell ringlet. Adjusting the polynomials used in the spline fit will alleviate this error, and it is up to the user to decide when the fit is sufficient for their needs.
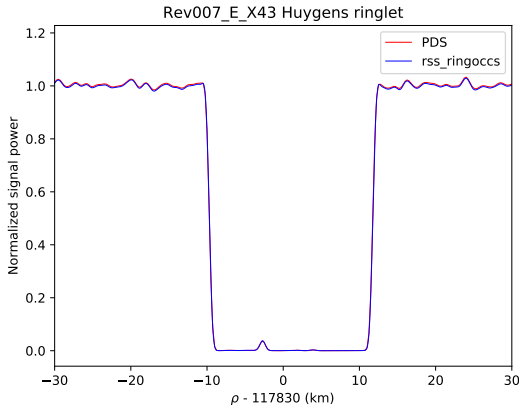


11.1: Huygens ringlet reconstructed normalized power.
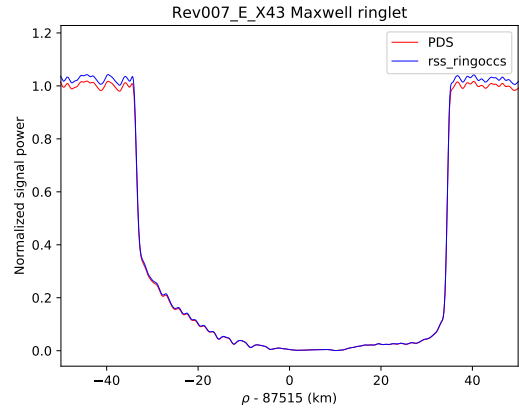
11.2: Maxwell ringlet reconstructed normalized power.

Fig. 11: Comparison of reconstructed normalized power with PDS results. PDS results are plotted in red and can be found from `Rev007/Rev007E/Rev007E_RSS_2005_123_X43_E/RSS_2005_123_X43_E_TAU_01KM.TAB`). `rss_ringoccs` results are in blue.

## 5.2 Effect of different sampling rates

The raw data recorded at the DSN stations are sampled at 16 kHz. The high resolution of these data poses two difficulties: (i) each RSR data file is at least many hundreds of MB

in size for an ingress or egress diametric occultation (chord occultations are even larger), which can be cumbersome especially for users downloading a large number of RSR files; (ii) the `rss_ringoccs` processing time on a conventional laptop for each data file can be at least thirty minutes for diametric occultation (even longer for chord occultations), which is particularly computationally expensive for users planning to reduce data for numerous occultations. The PDS provides RSR data files with the raw data down-sampled to 1 kHz. These files are twelve to sixteen times smaller (lower limit of tens of MB instead of hundreds) and take 90 to 180 seconds for `rss_ringoccs` to process.

The computational benefits of utilizing the 1 kHz files over the 16 kHz files is clear. However, we must demonstrate that the down-sampled data yield results comparable to those of the raw high-resolution data. To begin this validation, we process 1 kHz and 16 kHz data files for X band at high ring opening angle ($B \approx 23°$) and Ka band at low ring opening angle ($B \approx 5°$). Then, we compare and contrast the 1 kHz and 16 kHz processing results from the calibration, DLP, and reconstruction steps as shown in Fig. 12 at the end of this document.

The frequency offset and freespace power fits differ by less than 0.1% within the ring system, while the computed frequency offsets differ by less than 0.01%. The DLP optical depth values are typically within 0.01 dB of one another, although this is not the case for the part of the profile associated with the B ring. Any differences seen between the two profiles can be ascribed to changes in the diffraction pattern when the profile is down-sampled to the DLP radial sampling resolution. This assertion is substantiated by the similarity of the diffraction-corrected optical depth profiles. Because the diffraction reconstruction eliminates diffraction patterns in the profile, the excellent agreement of the two reconstructed profiles indicates that the disparity between the DLP optical depths is due to differences in the diffraction patterns.

Having been demonstrated to yield results comparable to those from the 16 kHz files for 1 km reconstructions, the 1 kHz files are recommended for processing instead of the 16 kHz files. Users can obtain 1 kHz files for the majority of occultations from the PDS with only a few exceptions. In these cases, we recommend the user decimate the 16 kHz file to 1 kHz at the start of the pipeline by setting the `decimate_16khz_to_1khz` keyword argument equal to `True`.

# 6 Voyager 2 Uranus occultation

The Voyager 2 X-band (3.6 cm) radio occultation of the Uranian rings on January 24-25, 1986 provides the highest resolution observations for the Uranian ring system to date. Definitive analysis of the Voyager 2 occultation was performed by Gresh et al. (1989) and the final results were archived at 50 m resolution. The best Earth-based Uranus ring occultation dataare diffraction-limited to 1-2 km, inhibiting detailed analysis of internal structure of the rings. The Voyager 2 RSS Uranus ring occultation SNR is high enough to push the diffraction-reconstructed resolution to 20 m to reveal more internal structure of the rings, opening up possibilities for new science. These observations provide a unique opportunity to demonstrate the applicability of the `rss_ringoccs` reconstruction software to contexts outside of the Cassini radio occultations of Saturn's rings with

readily-available validation of the results.

## 6.1 Changes to the procedure

While the procedure for processing the Voyager 2 radio occultation data is comparable to the approach taken by `rss_ringoccs` for the Cassini radio occultations, there are some key differences that required adapting some components of the default processing pipeline.

1. Voyager 2 RSS Uranus ring data are stored in binary files that are not formatted in the same manner as the RSR files for Cassini radio occultations stored on the PDS. This requires a unique file reader.

2. The imaginary component of the complex signal was not recorded and must be inferred from the real component.

3. The Uranian ring system is highly inclined with respect to the Earth. While enabling the high SNR necessary for high-resolution reconstruction, this changes the occultation geometry.

4. Each ring of Uranus has a different inclination and eccentricity, which requires separate treatment of the occultation geometry for each ring to accurately calculate the ring intercept radius in each ring frame (for the Saturnian rings, `rss_ringoccs` computes the geometry for Saturn's equatorial reference frame). This requires processing each ring individually.

5. The oscillator on board the Voyager 2 spacecraft did not possess the same quality or precision as the USO on board the Cassini spacecraft. This requires adjustments to the phase corrections using the frequency offset, as well as an additional step in detrending the systematic drift in signal phase.

6. Each ring is accompanied in both radial directions by substantial amount of free space power, which eliminates the need for gap finding but does require locally fitting for the free space power in the vicinity of each narrow ring.

7. Output file documentation, i.e., the LBL files, must be adapted to reflect the occultation observation information and processing history.

We provide an adaptation of our software with the v1.2 release of `rss_ringoccs` that addresses the majority of these issues.

### 6.1.1 Changes to reading raw data

The original Voyager 2 RSS Uranus ring occultation observations at X-band were recorded at 50 kHz on digital tapes when received by the DSN stations in Parkes and Canberra. They are not currently available on the PDS, but Dick Simpson (NASA/PDS) kindly transferred these data to CDs, and then to DVDs, which he provided to our team. To obtain the raw X-band data files that contain the Uranus ring events, submit a request to Dick French, reachable at rfrench@wellesley.edu.

We have designed an object class that, when instantiated, reads in the Voyger 2 RSS binary files from the local drive. The raw data contain only the real part of the complex

transmittance. To recover the complete complex signal, the Uranus file reader class uses a Hilbert transform to compute $Q$ from the real component $I$ stored in the binary file.

### 6.1.2 Changes to geometry

The `Geometry` class continues to utilize `spiceypy`; however, this requires a different set of the kernel reference files to compute the occultation geometry. Most of these kernel files are provided with the v1.2 release. Those not included are large ($> 100$ Mb) and are also not available from the PDS. These kernel files are available upon request from Dick French, reachable at rfrench@wellesley.edu.

What distinguishes the Uranus version of `Geometry` from that of `rss_ringoccs` is its processing of the occultation geometry for each ring in its own reference frame rather than the host planet's equatorial reference frame. The frame kernel for each ring accounts for the ring's inclination and nodal regression. This enables more accurate calculation of the ring intercept radius.

### 6.1.3 Changes to calibration

Modifications to the `Calibration` step to accommodate Voyager 2 Uranus RSS observations involved two components of the phase corrections. The frequency offset correction original to `rss_ringoccs` is estimated assuming that the frequency offset falls in a 300 Hz window centered on 0 Hz with 0.5 Hz resolution in the discrete Fourier transform. For the Voyager 2 Uranus ring occultation, the frequency offset drifts over a 500 Hz window centered on -11 kHz. Additionally, the ring locations can be calculated from pre-existing orbital parameters, allowing us to mask the frequency offset to exclude any effects of the rings on the computed frequency offset from the fit to the frequency offset. Fitting the frequency offset is done before processing each individual ring because the frequency offset is not ring specific. Fitting the frequency offset could not be done with a single polynomial because of a cusp that occurs in both the ingress and egress occultations. Our solution to this was to split the frequency offset data into two sets where the cusp occurs in SPM and fit each set separately. While Gresh et al. (1989) fit each set of frequency offset values with a second order polynomial, we find the frequency offset is better described by a ninth order polynomial.

Each ring is then corrected by means of the phase detrending function as described in §4.3. The oscillator on board Voyager 2 was not as stable as the USO on Cassini, and the default first-order phase correction used in `rss_ringoccs` is not sufficient. After each ring undergoes first-order phase correction and downsampling to 5 kHz (necessary for the desired 5 m DLP resolution for the Uranian rings), an additional phase correction is applied. First the phase is unwrapped to recover the phase drift. Due to noise and diffraction patterns present in the signal phase, the unwrapping is not always successful. Corrections to the phase unwrapping are made using parameters stored in an ancillary reference file `phase_unwrap_params.py`. We do not recommend that users add to, remove, or otherwise change these parameters, but users may do so at their own risk.

Once the unwrapping corrections are made, we convolve the unwrapped phase by with a 1 second boxcar kernel. This time-averaging is comparable to the Gresh et al. (1989) approach of applying a low-pass filter to the unwrapped phase to obtain a fit to the

regional drift in phase. Unlike the low-pass filter approach, our time-averaging does not fully preserve the diffraction pattern encoded in phase after subtracting the fit from the observed phase. This poses a problem because this diffraction pattern is necessary for reconstructing the original profile. To preserve the diffraction pattern, we fit a second-order polynomial to the time-averaged unwrapped phase adjacent to the ring profile (where the diffraction pattern occurs in the phase) and replace the time-averaged fit over the diffraction pattern with the polynomial estimate, effectively assuming the polynomial is characteristic of the phase drift present in the diffraction pattern. Finally, we subtract the total fit from the unwrapped phase to correct for the second-order drift. This produces phase profiles comparable to those shown in Gresh et al. (1989).

During our preliminary processing of the Voyager 2 data, we found that normalizing the power before resampling to radius (the default sequence in `rss_ringoccs` would sometimes result in an average normalized free space power other than unity. Performing the power normalization after resampling the data from observed event time to ring intercept radius eliminates this effect. After resampling the data to uniform sampling in radius, we mask out each ring region identified by orbital parameters along with an additional 15 km on either side of the profile to exclude the entire diffraction pattern from the fit. Then, we fit the free space power with a ninth order polynomial and divide the total diffraction-limited power by the fit to obtain the normalized diffraction-limited profile.

### 6.1.4 Changes to DLP

As in `rss_ringoccs`, the DLP step primarily entails interpolating the Geometry and Calibration results to the uniform sampling in ring intercept radius. Threshold optical depth is calculated using noise power estimated from the STFT of the phase-corrected freespace power. Then, the reconstruction window size is estimated for the highest reconstruction resolution (20 m in this case) and Fresnel scale calculated by Geometry. To ensure reconstruction of the total ring profile with several kilometers of baseline freespace on either side of the profile, we pad the ring DLP profile output with additional data on either side of the profile to account for the window size necessary for reconstructing the end points. Limiting output to this small range of profile power dramatically reduces processing time as well as the output file size.

### 6.1.5 Changes to diffraction reconstruction

The reconstruction routines remain unchanged from the v1.2 `rss_ringoccs` version of diffrec. The major differences are in the default inputs for calling the `DiffractionCorrection`. The `res_fac` is set to unity so that the reconstruction and processing resolutions are identical, consistent with the MTR86 approach used by Gresh et al. (1989). The Allan deviation is set to the $2 \times 10^{-13}$ value suggested by Gresh et al. (1989). The default processing window is set to a Kaiser-Bessel window with $\alpha = 2.5$.

## 6.2 Validation of Uranus processing

To validate our processing results, we compare ring reconstruction at 50 m to the 50 m reconstructions computed and archived by Gresh et al. (1989). In general, the diffraction-reconstructed ring profiles are in excellent agreement in detailed structure, effective reso-

lution, and even in the patterns of the free-space noise. We consider this to be a successful validation of our method for processing the raw Voyager 2 data. Thus, our reconstruction of the raw Voyager 2 data can be considered comparable to that of Gresh et al. (1989) and can be reliably used to produced profiles at higher resolutions.



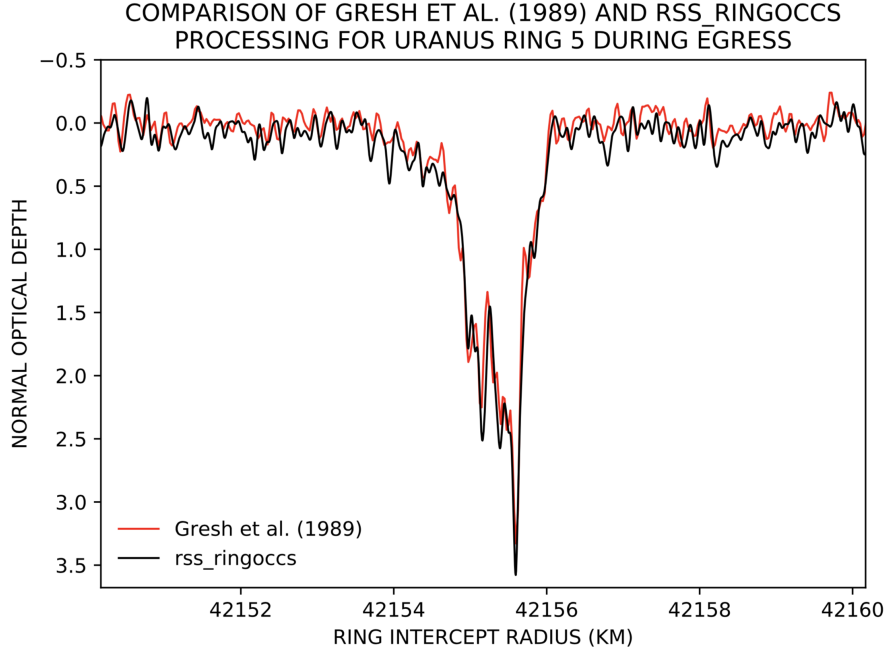Fig. 13: Comparison of our adapted `rss_ringoccs` processing of the Voyager 2 Uranus ring 5 egress occultation with that of Gresh et al. (1989).

Any disagreement between the Gresh et al. (1989) profiles and ours is small and could be attributed to several systemic differences. For example, Gresh et al. (1989) may not have recovered the imaginary component of the complex signal in the same manner as our pipeline. Their approach to phase corrections differs from ours and required three separate steps rather than two. It is also not explicitly clear which window function was used by Gresh et al. (1989) for their reconstruction. Finally, as of V1.2, our pipeline does not yet account for a elliptical ring geometry or a cant angle during the reconstruction.

# 7  Where to go from here

## 7.1  The Cassini RSS data catalog

We have created a CSV file (`data_catalog_V180806.csv`, located within the `tables` directory, listing all 1 kHz Cassini ring occultation RSR files available on the PDS. This catalog includes information of each RSR file, such as wavelength/frequency band, observing station information, sampling rate, associated kernels, etc., as well as relevant geometry parameters that can help users determine which file they want to use. The column headers and definitions for this catalog are also available within the `tables` directory in `data_catalog_definitions_V180806.txt`.

## 7.2    Selecting an RSR file to process

Before using `rss_ringoccs`, we recommend users browse the Cassini RSS data catalog to find an appropriate RSR file to process. Factors such as elevation angle, antenna size, ring radius range covered by the occultation, and ring opening angle can affect this decision.

First, users should establish that the RSR file covers the radius range of interest. Some occultations, such as chords, do not cover the entire ring system (see Figure 22.2). Next, depending on the research goal, users should select an observation with the desired ring opening angle. For high optical depth structure, a large ring opening angle is generally desirable, since it minimizes the slant path optical depth, whereas low ring opening angles are preferable for detecting vertical structure in the rings and probing tenuous material. Another factor to consider is the Earth receiving station. Different stations will record in different bands (S-, X-, or Ka-band) using different sized antennas (34 m or 70 m), affecting the SNR. The location of the DSN is also important, as Cassini could be lower in the sky when observed from one station than another – this affects the amount of atmosphere the signal must go through to reach the station. These station-related factors can affect the overall SNR as well as the background power drift.

## 7.3    Choosing a radial resolution

As discussed in Section 3.6, users must specify a desired radial resolution to `rss_ringoccs` in the form of radial sample spacing in km for both the DLP and the reconstructed profile. The latter must always be at least 8/3 greater than the former; however, there are additional considerations in choosing a sample spacing.

In Figure 8, Marouf et al. (1986) show a relation between threshold optical depth $\tau_{TH}$ (Section 4.4.1) and processing resolution $\Delta R$ for X and S band. Because lower resolutions lead to larger SNR values, $\tau_{TH}$ increases with $\Delta R$. If the intrinsic SNR is low–more often the case in Ka band or low-elevation observations with large Earth atmosphere extinction– a small radial sampling rate might not produce meaningful results because the profile normal optical depth frequently exceeds the threshold optical depth. In such cases, we recommend that users consider the threshold optical depth when specifying a desired resolution.

## 7.4    Execution time benchmarks

The single-file end-to-end example script discussed in §3.3 includes a benchmark computation time for a typical 1 kHz RSR file for a diametric occultation. When run, `e2e_run.py` will print out the expected processing time for a single 1 kHz RSR file. We have conducted a series of benchmarks for various machines across a range of hardware and operating systems and various resolutions. The results of these benchmark runs for a single 1 kHz file for Rev007 X-band at DSN-43 at X-band are listed below for reference. Note that processing time may vary based on other tasks being run by a machine at the time of running `rss_ringoccs`. For our own benchmarks, we find benchmark times can vary by up to ≈5% for a given machine.

| $\Delta\rho$ (km) | $4/3\Delta$R (km) | Time (s) |
|:---:|:---:|:---:|
| MacBook Pro, 2.9 GHz Intel Core i7, 16GB RAM | | |
| 0.25 | 1.0 | 90 |
| 0.25 | 0.667 | 120 |
| 0.05 | 0.25 | 270 |
| 0.05 | 0.134 | 400 |

Table 9: Benchmarks for processing the Rev 007 E X43 1 kHz RSR file.

In addition to these individual benchmarks, we have run a benchmark of the batch processing script. A complete run of `e2e_batch.py` which processes all 1 kHz RSR files before USO failure requires 5.25 hrs to run on with a 2.9 GHz Intel Core i7 CPU with 16 GB of RAM and $\approx$10 hrs with a 2.7 GHz Intel Core i5 CPU and 8 GB RAM.

## 7.5   Licensing

`rss_ringoccs` is free/open-source software made available under the GNU General Public License. The following license is included with the top-level `__init__.py` file in the `rss_ringoccs` software package:

```
Copyright (C) 2019 Team Cassini at Wellesley College

This program is free software: you can redistribute it
and/or modify it under the terms of the GNU General Public
License as published by the Free Software Foundation,
either version 3 of the License, or (at your option) any
later version.

This program is distributed in the hope that it will be
useful, but WITHOUT ANY WARRANTY; without even the implied
warranty of MERCHANTABILITY or FITNESS FOR A PARTICULAR
PURPOSE. See the GNU General Public License for more
details.

You should have received a copy of the GNU General Public
License along with this program. If not, see
http://www.gnu.org/licenses/.

This program is part of the rss_ringoccs repository hosted
at https://github.com/NASA-Planetary-Science/rss_ringoccs
and developed with the financial support of NASA's Cassini
Mission to Saturn.
```

## 7.6   Citing `rss_ringoccs`

If you use `rss_ringoccs` in your research as the basis of a publication, please consider citing the software package using the DOI:10.5281/zenodo.2548947

# Acknowledgements

# Appendices

## A    Meta-kernel file

A meta-kernel file contains a list of the complete pathnames to a list of individual kernel files. An example meta-kernel `Rev007_meta_kernel` has been provided in the `examples` directory for the Rev007 occultations. To create a meta-kernel for another occultation, follow the structure of the Rev007 meta-kernel example. Typically, the only files one needs to change are those with a `*.bsp` or `*.tpc` extension. All kernel files necessary for building the meta-kernel for a specific observation are listed in final column of the data catalog found in the `tables` directory. For example, the Rev014 occultation might have a meta-kernel with the following contents:

```
\begindata
PATH_VALUES = ( '../kernels/naif/CASSINI/kernels/spk'
               '../kernels/naif/CASSINI/kernels/lsk'
               '../kernels/naif/generic_kernels/spk/planets'
               '../kernels/naif/generic_kernels/spk/stations'
               '../kernels/naif/generic_kernels/pck'
               '../kernels/naif/CASSINI/kernels/pck'
               '../kernels/local')

PATH_SYMBOLS = ('A', 'B', 'C', 'D', 'E', 'F', 'G')

KERNELS_TO_LOAD = ( '$A/051011R_SCPSE_05245_05257.bsp'
                  '$B/naif0012.tls'
                  '$C/de430.bsp'
                  'F/cpck11Oct2005.tpc'
                  '$D/earthstns_itrf93_050714.bsp'
                  '$F/earth_000101_180919_180629.bpc')

\begintext
These are the kernels used for Rev014
```

## B    Calibration Output Plots

After computing $\hat{f}(t)_{offset}$ from the frequency offset, the `FreqOffsetFit` class plots $f(t)_{offset}$, the $f(t)_{offset}$ values used to compute $\hat{f}(t)_{offset}$, and $\hat{f}(t)_{offset}$, along with labels specifying the polynomial order used in the fit, information identifying the revolution number, direction, wavelength band, DSN station, processing date, and processing serial number. `FreqOffsetFit` saves this plot in a PDF in the subdirectory under `output` corresponding to the current Rev, band, and DSN station. This is the same directory as the `.LBL` and `.TAB` files output by `rss_ringoccs` if `write_file` is set to `True` (the recommended value). The output PDF is named following the same conventions as the `.LBL` and `.TAB` files, complete with processing date and serial number. We show an example of one such output plot in Figure 14 for the occultation Rev 007 in the egress direction as observed in the X-band from DSN station 43.
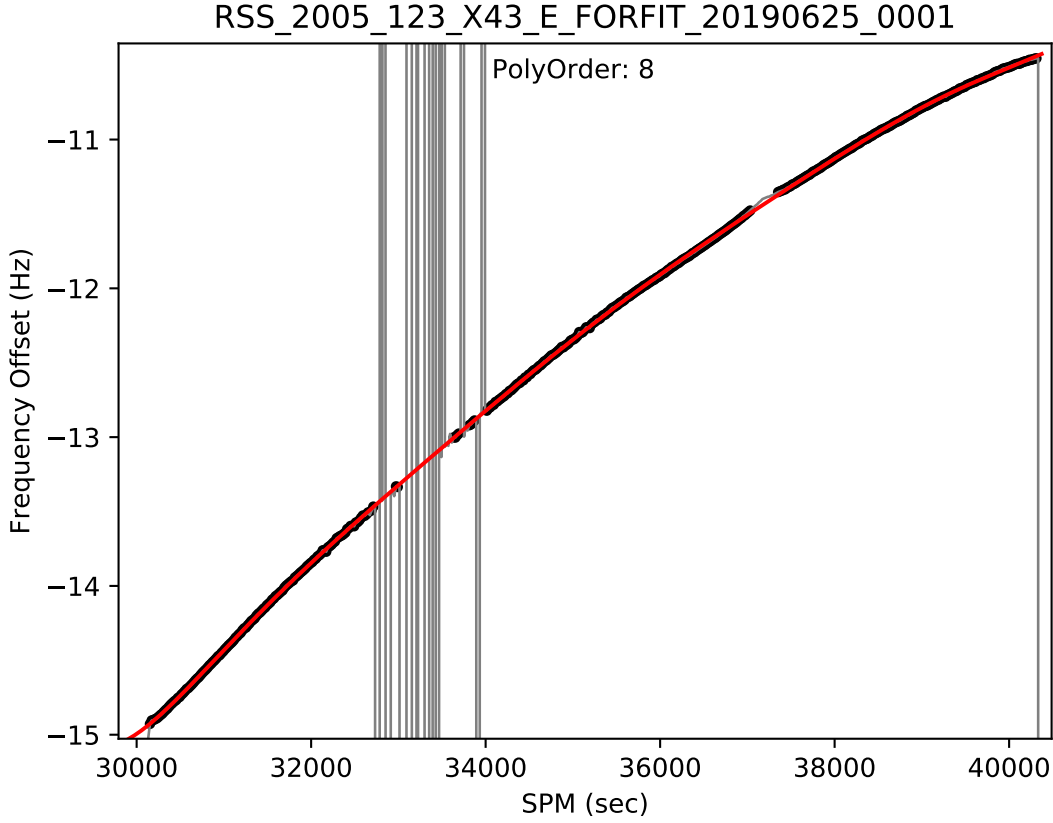
Fig. 14: Example of the frequency offset fit plot output by the `FreqOffsetFit` submodule of `Calibration` step. The total frequency offset $f(t)_{offset}$ is depicted in grey, the $f(t)_{offset}$ used to compute $\hat{f}(t)_{offset}$ in black, and the fit $\hat{f}(t)_{offset}$ in red.

After computing $\hat{P}_0$ from available freespace regions, the `Normalization` class plots power, the power values used to compute $\hat{P}_0$, and $\hat{P}_0$, along with labels specifying the fit type, fit order, and information identifying the revolution number, direction, wavelength band, DSN station, processing date, and processing serial number. `Normalization` saves this plot in a PDF in the subdirectory under `output` corresponding to the current Rev, band, and DSN station. This is the same directory as the `.LBL` and `.TAB` files output by `rss_ringoccs` if `write_file` is set to `True` (the recommended value). The output PDF is named following the same conventions as the `.LBL` and `.TAB` files, complete with processing date and serial number. We show an example of one such output plot in Figure 15 for the occultation Rev 007 in the egress direction as observed in the X-band from DSN station 43.

# C   Interactive Mode

When the `interact` keyword argument is set to `True` when instantiating the `Calibration` object class, the free space power fitting method will enter interactive mode to receive user input. After the initial automated fit to the free space regions, `rss_ringoccs` will plot the results of the fit (in the same manner as Figure 15) in a `matplotlib` window and prompt the user for input in the terminal.
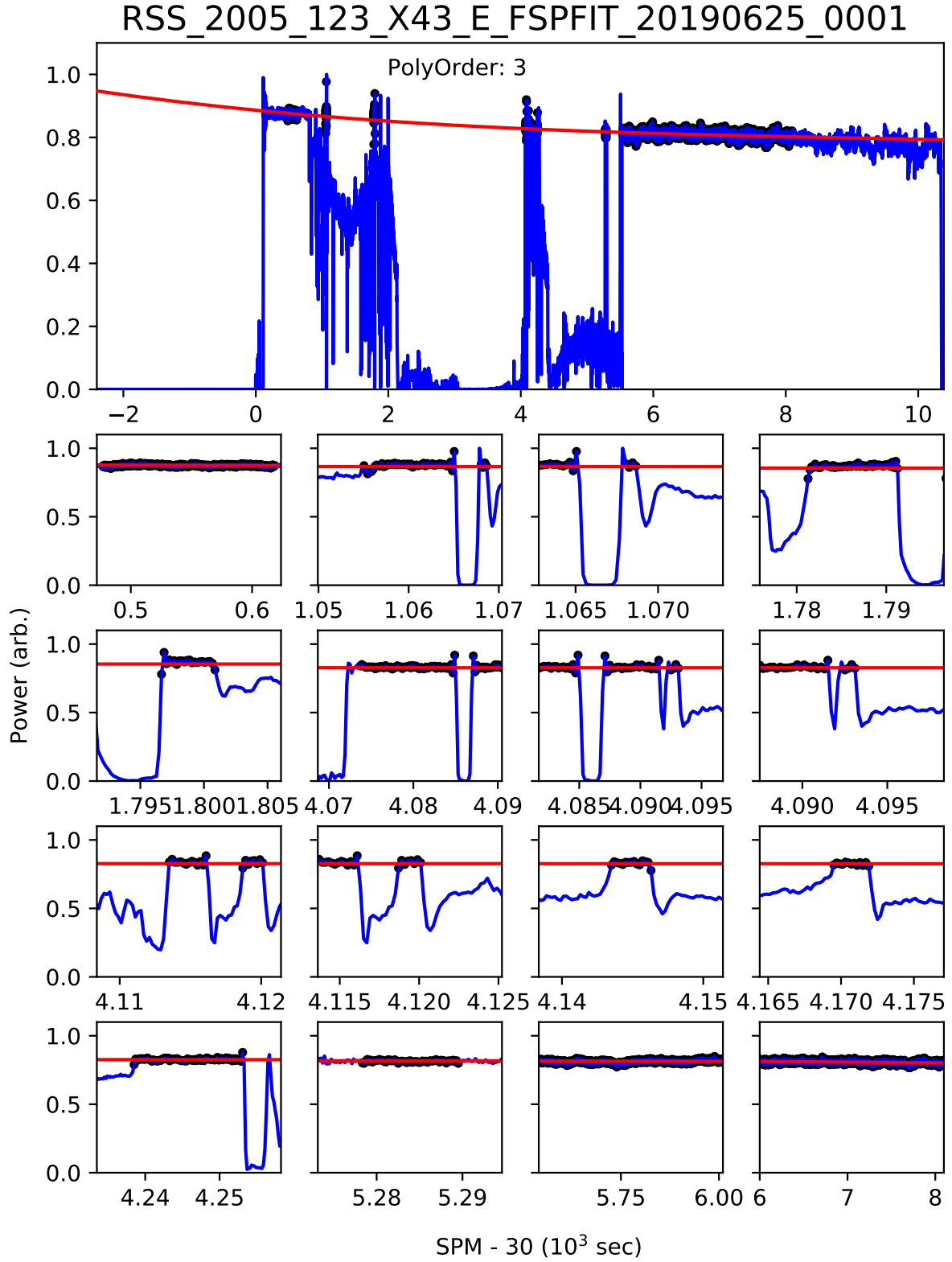
51

Fig. 15: Example of the free space power fit plot output by the `Normalization` submodule of `Calibration` step. Phase-detrended power is shown in blue, the power used to compute the fit $\hat{P}_0$ to the free space power in black, and the fit $\hat{P}_0$ in red. Top panel is the total power profile. Each subpanel is a closeup of one of the free space regions used in the fit. Subpanels shown in order of time observed (SPM). The number of subpanels will vary depending on the number of freespace regions used in the fit.

Here, we explain the input at each prompt and then show an example of a single iteration of the interactive mode with possible responses.

```
Do you want to continue with this fit? (y/n): n

Do you want to change the freespace regions? y


Last used freespace gaps in SPM:
[[30477.0, 30618.833698196322],
[31054.928062871928, 31065.345792559005],
[31067.770358800513, 31068.930045219375],
[31780.866566933848, 31791.436274129595],
[31796.580066071256, 31801.05616095102],
[34073.68113956013, 34085.4943434775],
[34086.68935725464, 34091.74708080809],
[34092.49215200969, 34093.327481330285],
[34113.3838723948, 34116.39786534125],
[34118.619852169526, 34120.21853934005],
[34143.358694145434, 34146.38873649045],
[34169.41951728726, 34172.05701601253],
[34238.49233676398, 34253.26244631217],
[35278.146362236446, 35289.59914281318],
[35545.59294280804, 36005.16144320606],
[36005.16144320606, 38092.48430556758]]


Do you want to revert to the default freespace gaps? n
Please input new freespace gaps in SPM and press enter twice:
[[30477, 30618],[31055, 31065],[34087, 34091],[34114, 34116],
[35546, 36005],[36006, 38092]]

[[30477, 30618],
[31055, 31065],
[34087, 34091],
[34114, 34116],
[35546, 36005],
[36006, 38092]]

What fit type would you like to use? (poly/spline): poly

What fit order would you like to use?: 3

Do you want to continue with this fit? (y/n): n
```

1. Entering y will end interactive mode and accept the current fit. Type n to continue interactive mode and change the fit properties.

2. n will skip the prompt for new free space regions. y will continue to the prompt for reverting to original free space regions.

3. y will revert the free space regions to those predicted by the Geometry class and skip the prompt for new free space regions. n will continue to a prompt for new, user-defined free space regions.

4. User now enters a 2xN list of floats specifying the desired free space regions in SPM (units of seconds). N must be greater than or equal to five in order for the free space fitting to properly select the data in the free space regions. For clarity and verification, the entered freespace regions will be printed to the terminal after the user input is parsed.

5. Enter the type of fit to use for the freespace power. Two fit types are available, a spline (`spline`) and a polynomial (`poly`); however, we highly recommend the polynomial fit.

6. Enter a whole number between 1 and 9 for polynomial fit or between 1 and 5 for spline fit.

7. A plot of the new fit made based on the user input will appear in a `matplotlib` window. The interactive mode will return to the initial prompt about whether to accept the fit or to continue with interactive mode. Return to step 1.
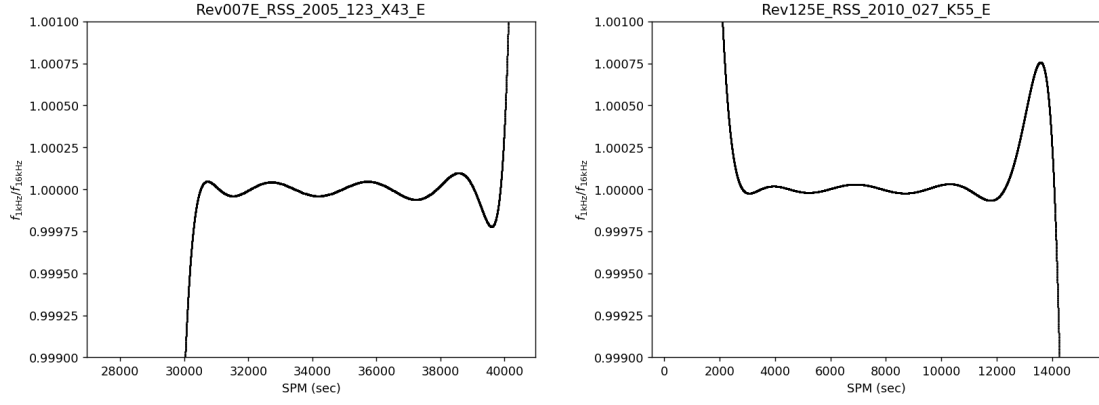
12.1: Ratio of 1 kHz to 16 kHz Frequency Offset Residual Fits.
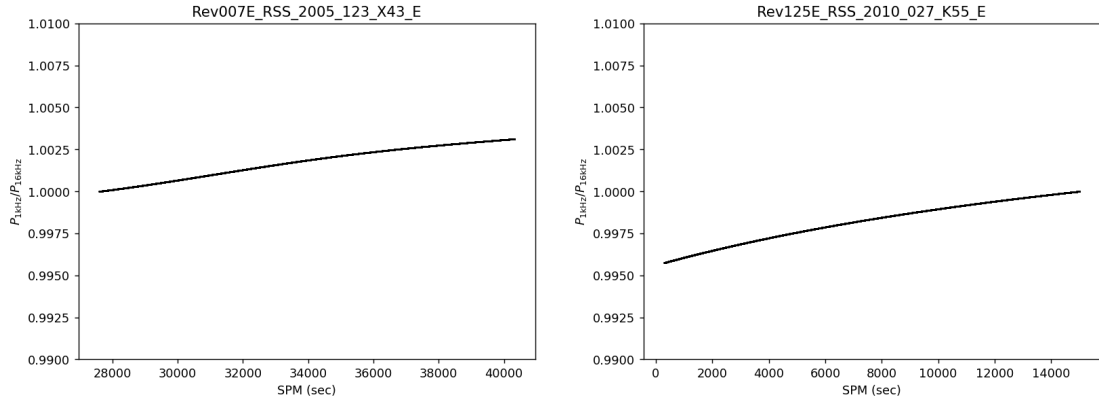


12.2: Ration of 1 kHz to 16 kHz Free Space Power Fits.
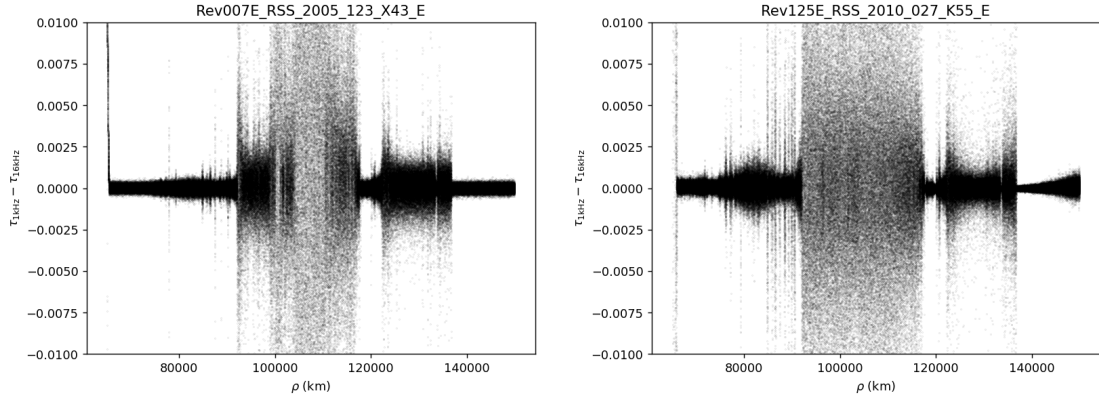


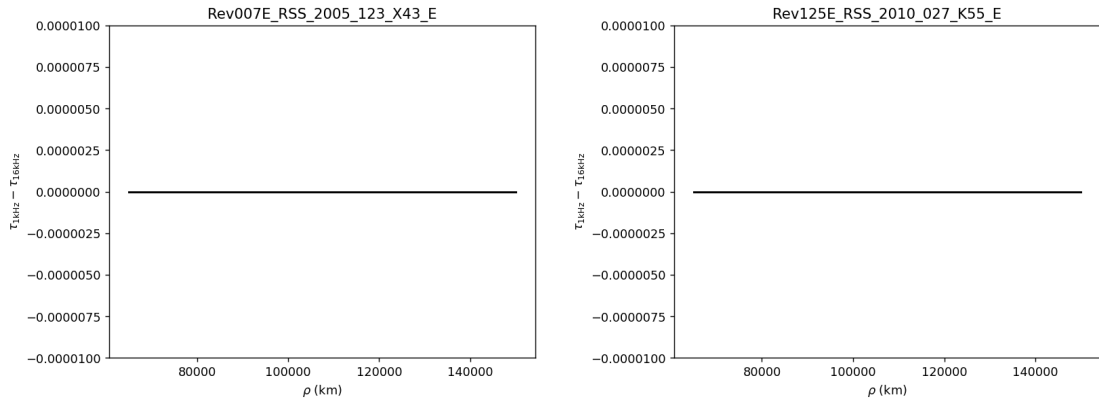12.3: Difference between 1 kHz and 16 kHz DLP optical depths.



Fig. 12: Validation of 1 kHz processing using raw 16 kHz processing for Rev 007 E X band and Rev 125 E Ka band.

# Acronyms

**DSN** Deep Space Network.

**HGA** High Gain Antenna.

**NASA** National Aeronautics and Space Administration.

**PDS** Planetary Data System.

**RSR** Radio Science Receiver.

**RSS** Radio Science Subsystem.

**SPM** Seconds Past Midnight.

# Glossary

**Atmospheric occultation**
Disappearance or reappearance of a source after the signal has passed through the atmosphere of a planet or satellite. 3

**Chord occultation**
Ring occultation. 4

**Deep Space Network**
NASA's complex of Earth-based antennas, used to communicate with spacecraft. 3

**Diametric occultation**
An occultation geometry in which the path of the complete occultation extends from ring ansa to ring ansa, passing behind the planet at mid-occultation. 3

**Diffraction Reconstruction**
Retrieval of radial optical depth profile of Saturn's rings responsible for observed diffraction pattern. 3

**Egress**
Exit phase of a ring or atmosphere occultation. 3

**Fresnel inversion**
Retrieval of intrinsic optical depth profile of the rings by using a Fresnel transform to correct for the effects of diffraction in the observed signal. 3

**High Gain Antenna**
Highly directional main spacecraft antenna for communications and radio science. 3

**Ingress**
Entry phase of a ring or atmosphere occultation. 3

**NASA**
National Aeronautics and Space Administration. 2

**Planetary Data System**
Long-term archive of digital data products returned from NASA's planetary missions, and from other kinds of flight and ground-based data acquisitions. 2

**Radio Science Receiver**
An open-loop receiver used in NASA's Deep Space Network (DSN) facilities. 4, 5

**Radio Science Subsystem**
A subsystem placed on board a spacecraft for radio science purposes. 2

**Rev number**
The number of times the Cassini spacecraft has orbited Saturn. 3

**SPM**
seconds past midnight. 25

# References

Acton, C. (1996), 'Ancillary Data Services of NASA's Navigation and Ancillary Information Facility', *Planetary and Space Science* **44**, 65–70.

Asmar, S. W., French, R. G., Marouf, E. A., Schinder, P., Armstrong, J. W., Tortora, P., Iess, L., Anabtawi, A., Kliore, A. J., Parisi, M., Zannoni, M., & Kahan, D. (2018), *Cassini Radio Science User's Guide*, v1.1 edn, NASA Jet Propulsion Laboratory.

Colwell, J., Nicholson, P., Tiscareno, M., Murray, C., French, R. & Marouf, E. (2009), 'The Structure of Saturn's Rings', *Saturn from Cassini-Huygens* p. 375.

French, R., McGhee-French, C., Lonergan, K., Sepersky, T., Jacobson, R., Nicholson, P., Hedman, M., Marouf, E. & Colwell, J. (2017), 'Noncircular features in Saturn's rings IV: Absolute radius scale and Saturn's pole direction', *Icarus* **290**, 14–45.

French, R., Nicholson, P., Hedman, M., Hahn, J., McGhee-French, C., Colwell, J., Marouf, E. & Rappaport, N. (2016a), 'Deciphering the embedded wave in Saturn's Maxwell ringlet', *Icarus* **279**, 62–77.

French, R., Nicholson, P., McGhee-French, C., Lonergan, K., Sepersky, T., Hedman, M., Marouf, E. & Colwell, J. (2016b), 'Noncircular features in Saturn's rings III: The Cassini Division', *Icarus* **274**, 131–162.

Gresh, D. L., Marouf, E. A., Tyler, G. L., Rosen, P. A. & Simpson, R. A. (1989), 'Voyager radio occultation by Uranus' rings I. Observational results', *Icarus* **78**(1), 131–168.

Kliore, A., Anderson, J., Armstrong, J., Asmar, S., Hamilton, C., Rappaport, N., Wahlquist, H., Ambrosini, R., Flasar, F., French, R., Iess, L., Marouf, E. & Nagy, A. (2004), 'Cassini Radio Science', *Space Science Reviews* **115**, 1–70.

Marouf, E., French, R., Rappaport, N., Wong, K., McGhee-French, C. & Anabtawi, A. (2011), 'Uncovering of small-scale quasi-periodic structure in Saturn's ring C and possible origin', *EPSC-DPS Joint Meeting* **265**.

Marouf, E., Tyler, L. & Rosen, P. (1986), 'Profiling Saturn's rings by radio occultation', *Icarus* **68**, 120–166.

Marouf, E., Tyler, L., Zebker, H., Simpson, R. & Eshleman, V. (1983), 'Particle Size Distributions in Saturn's Rings from Voyager 1 Radio Occultation', *Icarus* **54**, 189–211.

Moutamid, M. E., Nicholson, P., French, R., Tiscareno, M., Murray, C., Evans, M., French, C., Hedman, M. & Burns, J. (2016), 'How Janus' orbital swap affects the edge of Saturn's A ring?', *Icarus* **279**, 125–140.

Nicholson, P., French, R. & Colwell, M. H. E. M. J. (2014a), 'Noncircular features in Saturn's rings I: The edge of the B ring', *Icarus* **227**, 152–175.

Nicholson, P., French, R., McGhee-French, C., Hedman, M., Marouf, E., Colwell, J., Lonergan, K. & Sepersky, T. (2014b), 'Noncircular features in Saturn's rings II: The C ring', *Icarus* **241**, 373–396.

Rappaport, N., Longaretti, P., French, R., Marouf, E. & McGhee, C. (2009), 'A procedure to analyze nonlinear density waves in Saturn's rings using several occultation profiles', *Icarus* **199**.

Thomson, F., Marouf, E., Tyler, G., French, R. & Rappoport, N. (2007), 'Periodic microstructure in Saturn's rings A and B', *Geophysical Research Letters* **34**, L23203.